AEDC-TR-80-29

Skin-Friction Measurements at Subsonic and Transonic Mach Numbers with Embedded-Wire Gages

D. W. Sinclair
ARO, Inc.

January 1981

Final Report for Period October 1978 — March 1980

Approved for public release; distribution unlimited.

ARNOLD ENGINEERING DEVELOPMENT CENTER
ARNOLD AIR FORCE STATION, TENNESSEE
AIR FORCE SYSTEMS COMMAND
UNITED STATES AIR FORCE

NOTICES

When U. S. Government drawings, specifications, or other data are used for any purpose other than a definitely related Government procurement operation, the Government thereby incurs no responsibility nor any obligation whatsoever, and the fact that the Government may have formulated, furnished, or in any way supplied the said drawings, specifications, or other data, is not to be regarded by implication or otherwise, or in any manner licensing the holder or any other person or corporation, or conveying any rights or permission to manufacture, use, or sell any patented invention that may in any way be related thereto.

Qualified users may obtain copies of this report from the Defense Technical Information Center.

References to named commercial products in this report are not to be considered in any sense as an indorsement of the product by the United States Air Force or the Government.

This report has been reviewed by the Office of Public Affairs (PA) and is releasable to the National Technical Information Service (NTIS). At NTIS, it will be available to the general public, including foreign nations.

APPROVAL STATEMENT

This report has been reviewed and approved.

Elton R Thompson

ELTON R. THOMPSON
Directorate of Technology
Deputy for Operations

Approved for publication:

FOR THE COMMANDER

Marion L. Laster

MARION L. LASTER
Director of Technology
Deputy for Operations

REPORT DOCUMENTATION PAGE

READ INSTRUCTIONS BEFORE COMPLETING FORM

1 REPORT NUMBER
AEDC-TR-80-29

2 GOVT ACCESSION NO.

3 RECIPIENT'S CATALOG NUMBER

4 TITLE (and Subtitle)
SKIN-FRICTION MEASUREMENTS AT SUBSONIC AND TRANSONIC MACH NUMBERS WITH EMBEDDED-WIRE GAGES

5 TYPE OF REPORT & PERIOD COVERED
Final Report, October 1978 - March 1980

6. PERFORMING ORG. REPORT NUMBER

7 AUTHOR(s)
D. W. Sinclair, ARO, Inc.,
a Sverdrup Corporation Company

8. CONTRACT OR GRANT NUMBER(s)

9 PERFORMING ORGANIZATION NAME AND ADDRESS
Arnold Engineering Development Center/DOT
Air Force Systems Command
Arnold Air Force Station, TN 37389

10 PROGRAM ELEMENT, PROJECT, TASK AREA & WORK UNIT NUMBERS
Program Element 65807F

11. CONTROLLING OFFICE NAME AND ADDRESS
Arnold Engineering Development Center/DOS
Air Force Systems Command
Arnold Air Force Station, TN 37389

12. REPORT DATE
January 1981

13. NUMBER OF PAGES
44

14 MONITORING AGENCY NAME & ADDRESS(if different from Controlling Office)

15. SECURITY CLASS (of this report)
UNCLASSIFIED

15a DECLASSIFICATION/DOWNGRADING SCHEDULE
N/A

16 DISTRIBUTION STATEMENT (of this Report)
Approved for public release; distribution unlimited.

17 DISTRIBUTION STATEMENT (of the abstract entered in Block 20, if different from Report)

18 SUPPLEMENTARY NOTES
Available in Defense Technical Information Center (DTIC).

19 KEY WORDS (Continue on reverse side if necessary and identify by block number)

skin friction	bodies of revolution
gages	shear stress
transonic flow	electrical resistance
boundary layer flow	temperature sensitive elements
thermocouples	

20 ABSTRACT (Continue on reverse side if necessary and identify by block number)

Embedded-wire skin-friction gages were tested in the Acoustic Research Tunnel (ART) and on a model in Tunnel 16T at AEDC. The range of Mach numbers and Reynolds numbers considered was typical of the conditions encountered in transonic wind tunnel testing. Data obtained by the embedded-wire technique agreed well with data from conventional methods of measuring skin friction when the gages were calibrated in situ. When the gages were calibrated and

DD FORM 1 JAN 73 1473 EDITION OF 1 NOV 65 IS OBSOLETE

20. ABSTRACT (Continued)

reinstalled at a later date, the calibration coefficients could not be corrected by simple techniques.

AFSC
Arnold AFS Tenn

PREFACE

The work reported herein was conducted by the Arnold Engineering Development Center (AEDC), Air Force Systems Command (AFSC). The experimental results presented herein were obtained by ARO, Inc., AEDC Division (a Sverdrup Corporation Company), operating contractor for the AEDC, AFSC, Arnold Air Force Station, Tennessee. The experimental research was conducted under ARO Project Numbers P32L-01E, P32G-23C, P41T-A2, and P41T-E7. The data analysis was completed in April 1980, and the manuscript was submitted for publication on July 1, 1980. The AEDC project manager was Elton R. Thompson.

CONTENTS

Page

1.0 INTRODUCTION 5
2.0 APPARATUS
2.1 Test Facilities 6
2.2 Test Article 9
2.3 Instrumentation 14
3.0 PROCEDURES
3.1 Calibration 18
3.2 Data Acquisition 21
3.3 Data Reduction 22
3.4 Data Uncertainty 24
4.0 RESULTS
4.1 Experiments in the ART (Phase I) 27
4.2 Experiments in Tunnel 16T (Phase II) 32
5.0 CONCLUSIONS 39
REFERENCES 40

ILLUSTRATIONS

Figure

1. Acoustic Research Tunnel (ART) 7
2. Embedded-Wire Gage Installation in the ART 8
3. Model Installation in Tunnel 16T 9
4. EBOR Model Installed in Tunnel 16T 10
5. Test Article and Dimensions 11
6. Embedded-Wire Gage 14
7. Embedded-Wire Control Circuit 15
8. Preston Tube Installation on EBOR Model 17
9. Boundary-Layer Rake Installation on EBOR Model 18
10. Typical Calibration Curve for an Embedded-Wire Gage 19
11. Typical Embedded-Wire Shear Stress Calibration 20
12. Estimate of the Uncertainty in the Free-Stream Mach Number for the ART 25
13. Estimated Uncertainties in Wind Tunnel Parameters for Tunnel 16T 26
14. Repeat Temperature-Resistance Calibration of an Embedded-Wire Gage 28
15. Comparison of Skin-Friction Coefficient from Preston Tube and Boundary-Layer Profile Measurements 29
16. Effect of Operating Temperature on the Embedded-Wire Calibration 30

Figure Page

17. Calibration Repeatability 30
18. Comparison of Repeated Measurements of Skin-Friction Coefficient in the ART ... 31
19. Comparison of Temperature-Resistance Curves for Repeat Calibration of a Single Embedded-Wire Gage 31
20. Measured and Calculated Local Skin Friction on the EBOR Model 33
21. Repeated Embedded-Wire Measurements 36
22. Total Skin-Friction Drag Coefficients at Mach Number 0.6 37
23. Total Skin-Friction Drag Coefficients at Unit Reynolds Number 3.35 x 10^6/ft 38
24. Uncalibrated Local Skin-Friction Parameter versus Reynolds Number Based on Distance from Nose of the EBOR Model 39

TABLES

1. Location of Instrumentation on the EBOR Model 12
2. Test Matrix for EBOR Model 22
3. Measurement Uncertainties 27

NOMENCLATURE 42

1.0 INTRODUCTION

The contribution of skin-friction to the total drag of a model is usually estimated from measurements of the total drag and the integrated pressure drag. The distribution of the skin-friction force on the model surface cannot be determined from such measurements, but must be determined by measurements of the local shear stress on the model. The measurement of local skin-friction force is important in evaluating the contribution of the individual model components to the total skin-friction drag.

For many years, researchers have used the floating element balance to measure local skin friction. This balance is weight calibrated and measures shear stress directly, but its application to measurements on a wind tunnel model is difficult. Balances are usually bulky, and they cannot be mounted in small models or near the leading edge of large models. Also, shear stress balances are affected by pressure gradients and model vibration.

Local shear stress can also be determined from measurements of boundary-layer total pressure profiles. However, the probe traversing mechanism is bulky and difficult to mount on models with a small cross-sectional area, the time required to traverse the boundary layer is long, and the probe protrudes from the model surface so measurements cannot be made directly downstream of the probe. The boundary-layer total pressure rake eliminates this bulky mechanism and the long data acquisition time, but it introduces interferences which affect the measurement. Also, the number of measurement points in the boundary layer are diminished by the size and spacing requirements of the tubing used in its construction. Further, boundary-layer rakes are restricted to measurements in thick boundary layers.

Surface pressure probes such as Stanton tubes and Preston tubes protrude slightly from the model surface. Their presence disturbs the flow less than traversing probes or boundary-layer rakes, but the use of surface pressure probes still prohibits simultaneous measurements downstream of the probe location. In addition, their application is restricted by the pressure lag in the small diameter tubing required to make measurements in thin boundary layers. Consequently, it is extremely difficult to make measurements near the leading edge of a model.

Heat-transfer measurements can be used to determine skin friction through the application of Reynolds analogy. Gardon and thermopile gages have been used to measure the heat flux from wind tunnel models. These gages mount flush to the surface and do not have bulky hardware that must be mounted in the model. The major disadvantage of the Gardon and thermopile gages is that a driving temperature is required and measurements cannot be made at adiabatic wall conditions. Another device for measuring surface heat flux

is the heated-element gage which, unlike Gardon and thermopile gages, can be applied to measurements at adiabatic wall conditions. In addition, this gage is nonintrusive, its hardware is durable, data acquisition time is reasonably short, and with proper design, it is unaffected by pressure gradients. The addition of heat may have a destabilizing effect on a laminar boundary, but with care, the measurement of transition location is also possible. For these reasons, the heated-element gage appears attractive for measurements of local skin friction on wind tunnel models.

The heated-element gage was first suggested and evaluated by Ludwieg (Ref. 1), and refined by Liepmann and Skinner (Ref. 2), Bellhouse and Schultz (Ref. 3), Rubesin, et al. (Ref. 4), and Murthy and Rose (Ref. 5). In the present experimental study, the gage design presented by Rubesin, et al. (Ref. 4) was used. The purpose of the study was to investigate the use of heated-element (embedded-wire) measurements to obtain local skin-friction data on models tested in Tunnel 16T. The experimental program was conducted in two phases. The embedded-wire technique for obtaining skin friction was demonstrated in the Acoustic Research Tunnel (ART) during the first phase, and the technique was applied to measurements on a model in Propulsion Wind Tunnel (16T) during the second phase.

2.0 APPARATUS

2.1 TEST FACILITIES

2.1.1 Acoustic Research Tunnel (Phase I)

The Acoustic Research Tunnel (ART) is an open-circuit, atmospheric indraft tunnel that is connected to the Plenum Evacuation System (PES) of Tunnel 16T. The tunnel has a converging nozzle with a contraction ratio of 16, a 6-in.-square test section that is 24-in. long, and a 5-deg diffuser (Fig. 1). The top and bottom wall angle can be varied from -0.5 to 0.5 deg, and wall inserts are available to provide various wall porosities. Mach numbers from 0.05 to 1.10 can be generated in the ART when ventilated test section walls and wall divergences are used; however, the use of solid walls and a constant-area test section limits the maximum Mach number to 0.85. Further details of the ART can be found in Ref. 6.

During Phase I of the experimental program, solid wall inserts were installed in the ART and shear stress measurements were made on the floor of the test section at an axial location 14.375 in. from the test section entrance. This axial location was selected because boundary-layer profile measurements were previously made at this location from which skin friction could be calculated for comparison with the present data. The arrangement of the instrumentation is presented in Fig. 2. The instrumentation consisted of an embedded-wire gage, a copper-constantan thermocouple to measure wall temperature, a static pressure orifice, and a Preston tube used as a calibration standard.

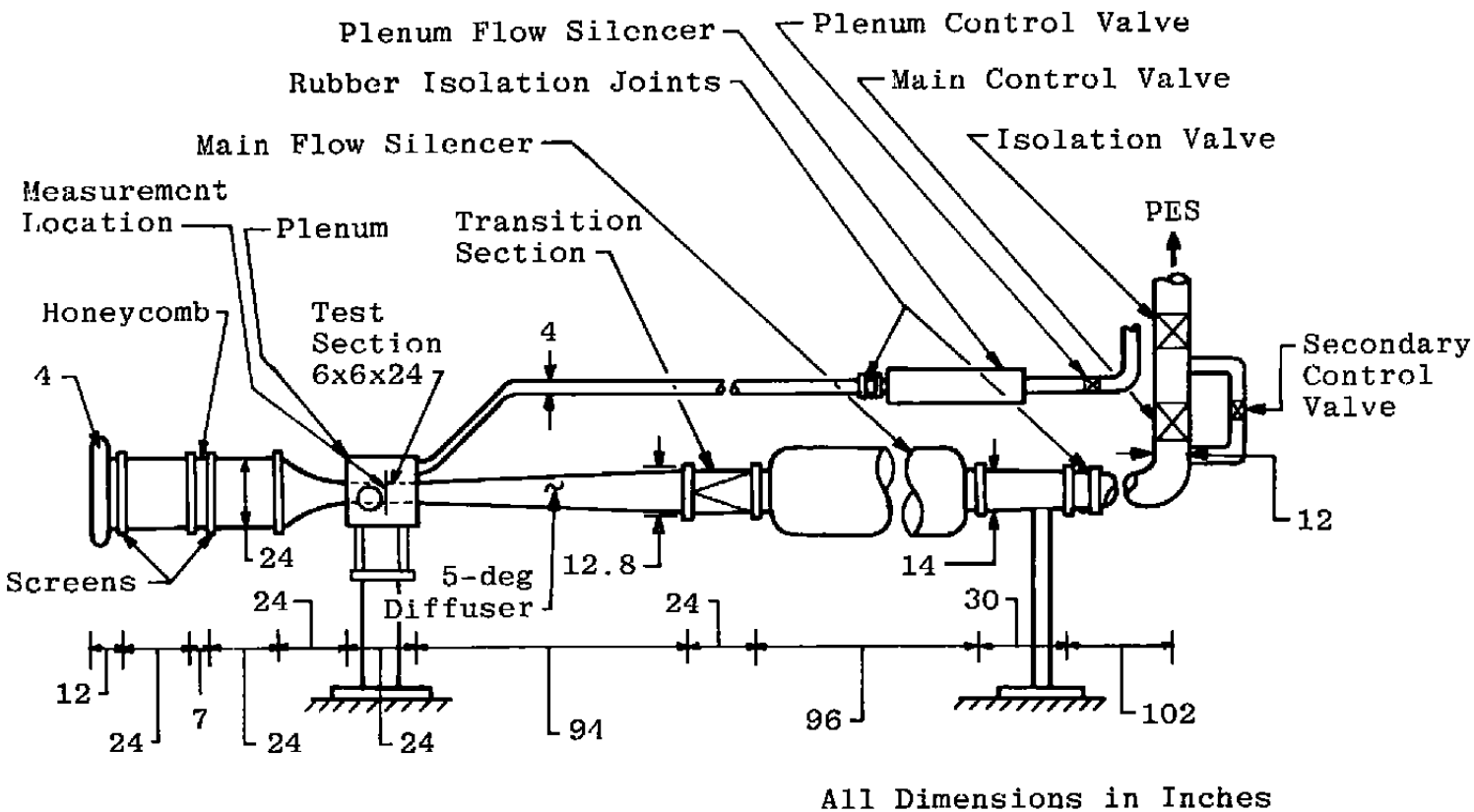

Figure 1. Acoustic Research Tunnel (ART).

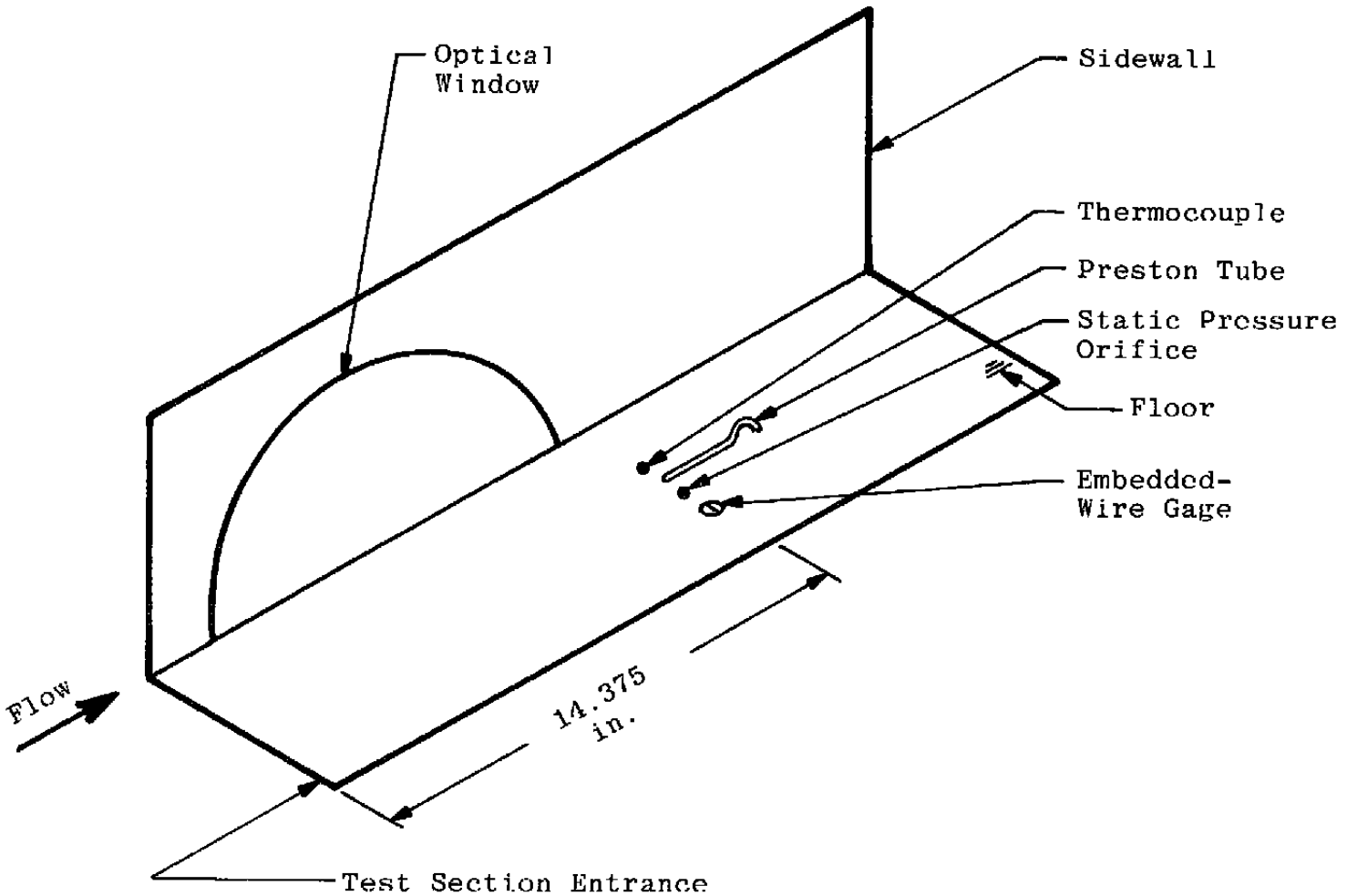

Figure 2. Embedded-wire gage installation in the ART.

2.1.2 Tunnel 16T (Phase II)

The AEDC Propulsion Wind Tunnel (16T) is a variable density, continuous-flow tunnel capable of being operated at Mach numbers from 0.2 to 1.5 and stagnation pressures from 120 to 4,000 psfa. The maximum attainable Mach number can vary slightly, depending upon the tunnel pressure ratio requirements with a particular test installation. The maximum stagnation pressure attainable is a function of Mach number and available electrical power. The tunnel stagnation temperature can be varied from about 80 to 160°F, depending upon the available cooling water temperature. The test section is 16-ft square by 40-ft long and is enclosed by 60-deg inclined-hole perforated walls of six-percent porosity. The general arrangement of the test section with the test article installed is shown in Fig. 3. Additional information about the tunnel, its capabilities, and operating characteristics is presented in Ref. 7.

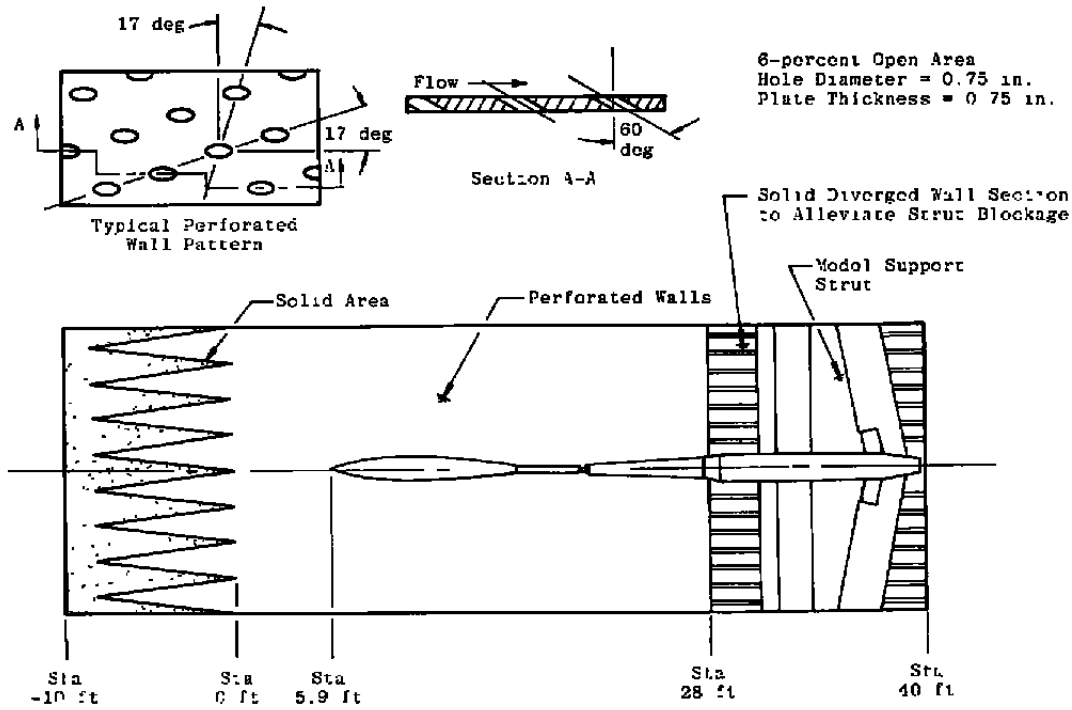

Figure 3. Model installation in Tunnel 16T.

2.2 TEST ARTICLE

A model was not required for the experiments performed in the ART. For the tests in Tunnel 16T, skin-friction measurements were made on an axisymmetric equivalent body of

revolution (EBOR) which represented the cross-sectional area distribution of a typical twin engine jet fighter. The sting-supported model is shown installed in the Tunnel 16T test section in Fig. 4, and the pertinent dimensions are presented in Fig. 5.

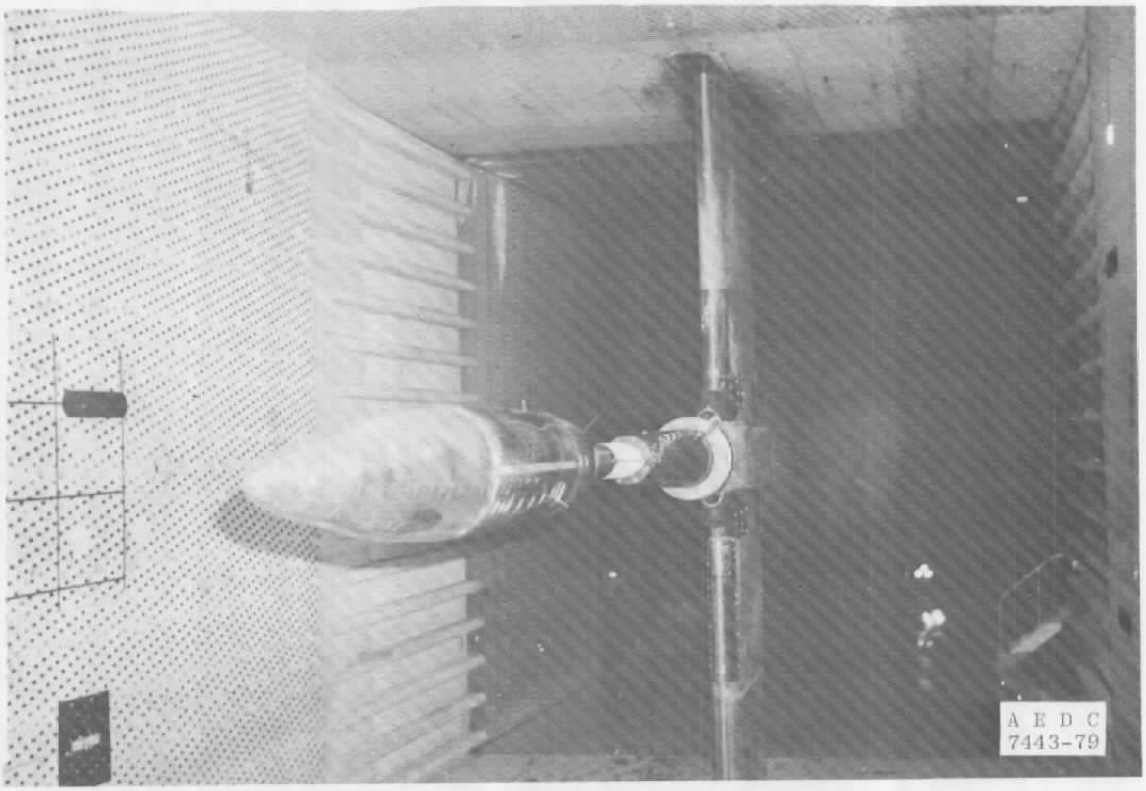

Figure 4. EBOR model installed in Tunnel 16T.

The model was instrumented to measure skin friction by several methods. The total skin-friction force was estimated from measurements of total axial force and integrated pressure drag. A six-component strain-gage balance was used to measure the axial force on the model, and integrated pressure drag was determined from 176 model surface static and four cavity pressures. Local skin-friction coefficients were determined from Preston tube and boundary-layer rake measurements. The location and dimensions of the nine Preston tubes and four boundary-layer rakes are presented in Table 1.

All model pressures were measured with a six-module scanning valve system using 15-psid transducers. The 48-port valves were controlled by a facility computer in a step-pause mode which monitored each pressure to ensure stabilization before advancing to the next port.

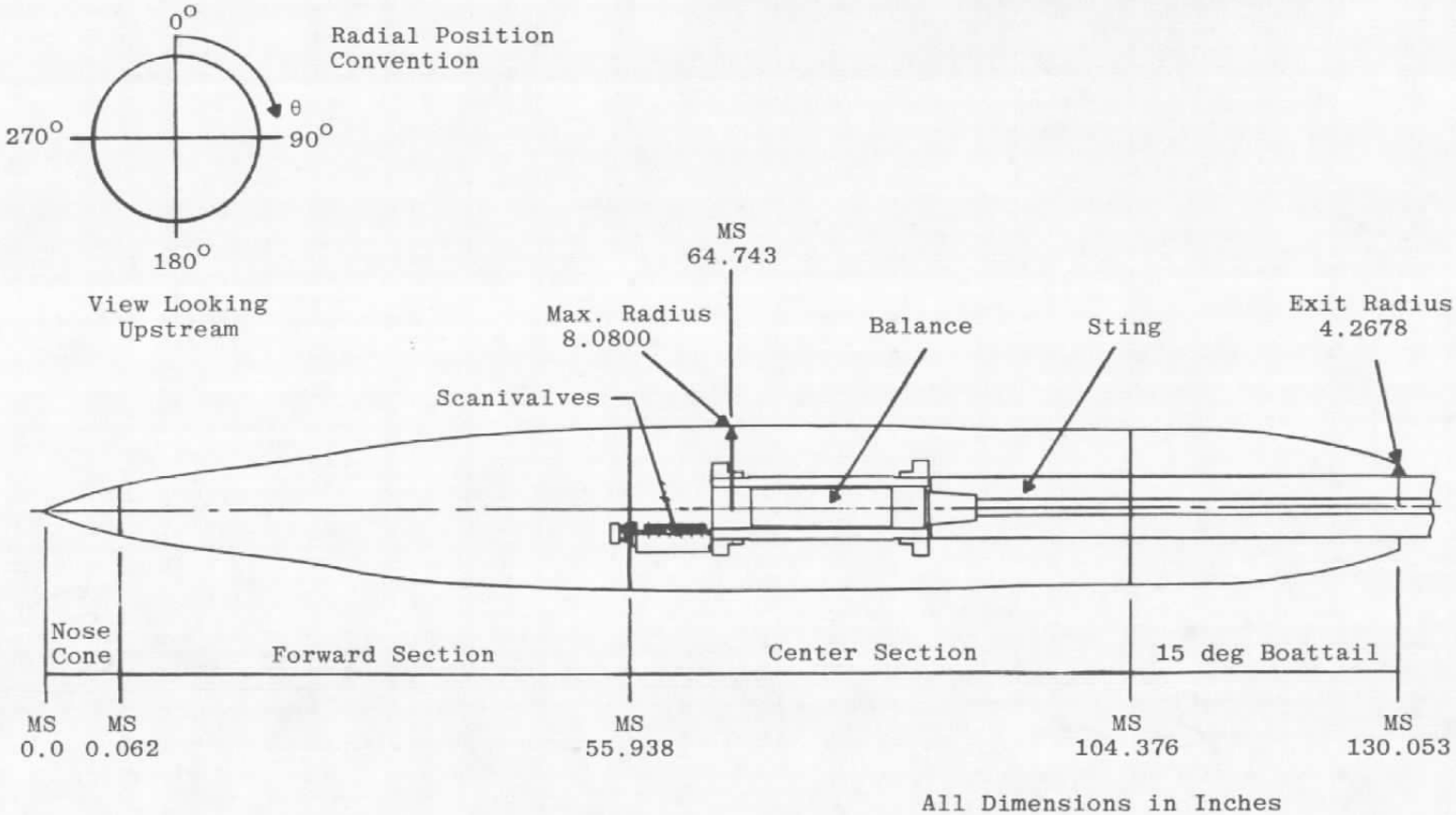

Figure 5. Test article and dimensions

Table 1. Location of Instrumentation on the EBOR Model

Model Station, in.	x/L	Embedded-Wire Gages	θ, deg	Copper-Constantan Thermocouples	θ, deg	Preston Tubes	θ, deg	Boundary-Layer Rakes	θ, deg
4,000	.031	2	225						
6,000	.046	3							
8,000	.062	4							
10,000	.077	5		2	210				
14,000	.108	7							
16,000	.123	8							
18,000	.138	9							
20,000	.154	10		3	210				
22,000	.169	11							
24,000	.185	12							
26,049	.200					1	5		
28,000	.215	14							
30,000	.231	15		4	210				
32,000	.246	16							
39,338	.302					2	275		
40,000	.308	18		5	210				
44,000	.338	19							
50,000	.384			6	210				
52,028	.400					3	95		
60,000	.461	23	45	7	30				
60,231	.463					4	265		
64,000	.492	24							

Table 1. Concluded

Model Station, in.	x/L	Embedded-Wire Gages	θ, deg	Copper-Constantan Thermocouples	θ, deg	Preston Tube	θ, deg	Boundary-Layer Rakes	θ, deg
70,000	.538		45	8	30				
72,000	.554	26							
76,000	.584	27							
80,000	.615	28		9	30				
84,582	.650					5	355		
88,000	.677	30							
90,000	.692			10	30				
91,348	.702					6	265		
92,000	.707	31							
94,731	.728							1	247.5
96,000	.738	32							
100,000	.769			11	30				
103,743	.798					7	95		
104,000	.800	34							
106,048	.815							2	22.5
108,000	.830	35							
110,000	.846			12	30				
112,000	.861	36							
113,828	.875							3	112.5
116,000	.892	37							
117,207	.901					8	355		
120,000	.923	38							
121,597	.935							4	337.5
124,000	.953	39							
125,209	.963					9	275		
128,000	.984	40		14	30				

The model was originally configured with 40 embedded-wire skin-friction gages and 14 copper-constantan thermocouples. Following installation and test, 30 of the embedded-wire gages and 12 thermocouples had survived. Locations of the embedded-wire gages and copper-constantan thermocouples are presented in Table 1.

2.3 INSTRUMENTATION

2.3.1 Embedded-Wire Gages

A schematic of the embedded-wire gages is presented in Fig. 6. The design is similar to the one used by Rubesin, et al. (Ref. 4) and Murthy and Rose (Ref. 5). The basic design

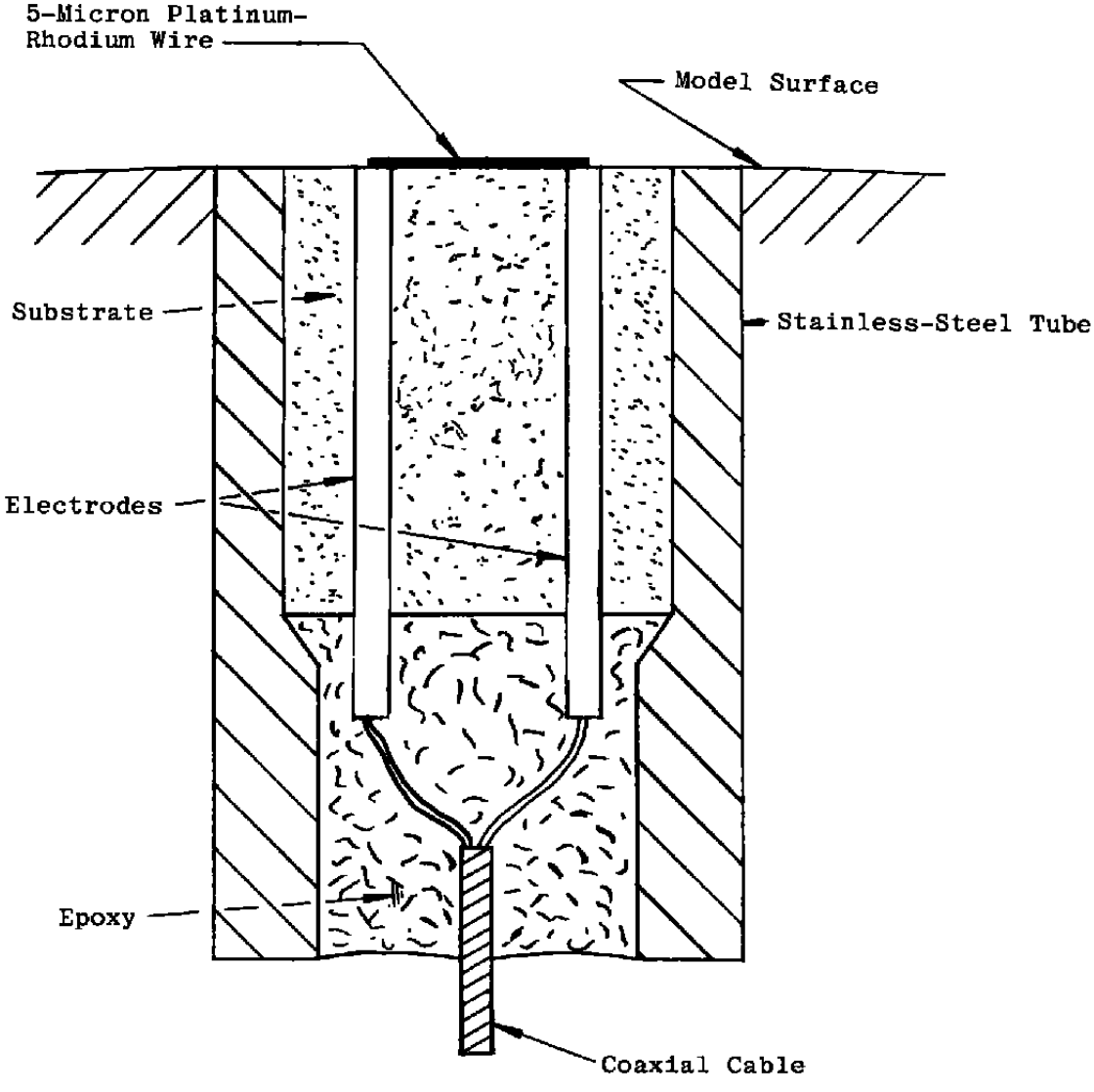

Figure 6. Embedded-wire gage.

parameters for determining the physical dimensions of the gages are presented in Ref. 4. The gage consists of a pair of nickel electrodes molded in a polystyrene substrate. During their construction, a coaxial cable is soldered to the electrodes, the substrate is expoxied into a stainless-steel tube, a thin platinum-rhodium wire is welded to the electrodes on the surface of the gage, and finally, a volatile solvent is applied to the gage surface to dissolve the substrate material. When the solvent evaporates, the wire has become coated with substrate material and thus is embedded in the gage surface. All gages were constructed by this technique. The only variation in the gage construction was in the diameter of the platinum-rhodium wire used. During Phase I, 5- and 10-μm wire was used. From the initial experimental results the 5-μm wire was selected for measurements on the EBOR model in Tunnel 16T.

The embedded-wire gages were operated in a constant temperature mode in which the power supplied to the gages is adjusted to maintain them at a constant operating temperature. A constant temperature corresponds to a constant resistance. Gage temperature is usually controlled by a commercially available constant temperature hot wire anemometer system, but these systems are expensive and the cost is prohibitive if many data channels are required. Although it lacked the frequency response of a commercial anemometer, a simple control system was designed and fabricated for this project. A schematic of the system is presented in Fig. 7. The system measures the current through the

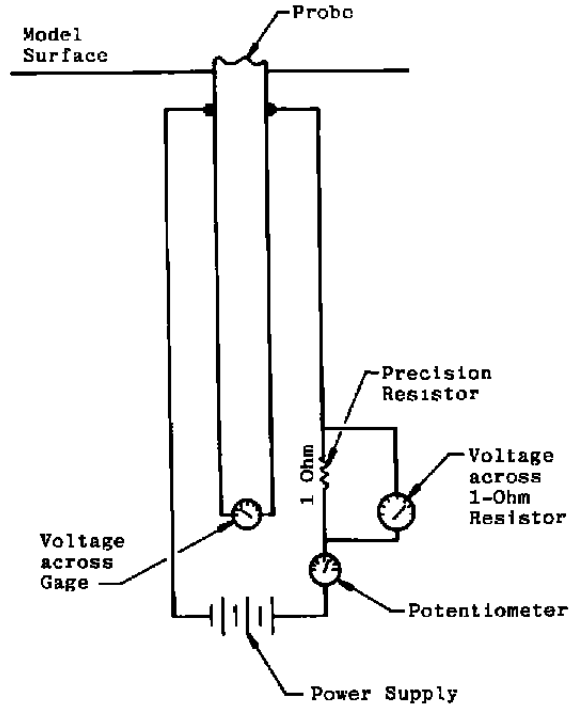

Figure 7. Embedded-wire control circuit.

voltage across the gage. The current through the gage is determined by measuring the voltage across a precision 1-ohm resistor connected in series with the gage. The current through the precision resistor is the same as the current through the gage and is equal to the voltage across the resistor divided by the resistance. The voltage across the gage is measured by a separate set of sensing leads from the control panel to the gage. The circuit enables steady-state measurements of the power supplied to the gage and the resistance of the gage to be made. In the resistance measure mode, a small current is supplied to the gage, and the voltage across the gage and the current through the gage are measured. The ratio of the voltage over current is the gage resistance. The small current applied to the gage in the resistance measure mode will not heat the gage significantly. Thus, the resistance measured is the cold resistance of the gage at the wall temperature. In the operating mode, the current to the gage is adjusted using the potentiometer. A preselected value of the gage resistance (gage temperature) is set and the power required to maintain the selected resistance is measured.

Measurements using this circuit are independent of line length and temperature gradient along the wire. This was an important requirement for the measurement system because the line length required in Tunnel 16T and the temperature difference expected between wind-off and wind-on conditions could change the resistance of the instrument leads by as much as 50 percent of the gage cold resistance. Such resistance changes would introduce a significant error, making accurate measurements by the embedded-wire technique impossible.

2.3.2 Preston Tubes

A Preston tube is a circular pitot tube mounted flush to a surface as shown in Fig. 8. The Preston tubes for this project were constructed from stainless-steel tubing with a ratio of inside to outside diameter equal to 0.6. The required outside diameter of each Preston tube was determined by applying the criteria presented by Preston (Ref. 8) to the range of boundary-layer thicknesses expected at each measurement location. Estimates of the range of boundary-layer thickness expected in the ART were determined from measurements reported by Benek (Ref. 9). The boundary-layer characteristics for the EBOR model were calculated using the Shear-Work-Integral-Method (SWIM) computer code developed by Whitfield (Ref. 10). Pressure distributions measured on the EBOR model and reported by Spratley (Ref. 11) were input to the SWIM code. From this information, a 0.032-in.-OD tube was selected for the experiments in the ART, and the tube diameters and measurement locations presented in Fig. 8 were selected for the EBOR model. More recent Preston tube design criteria presented by Patel (Ref. 12) and Allen (Ref. 13) indicate that tubing with a much larger diameter could have been used without influencing the accuracy of the data.

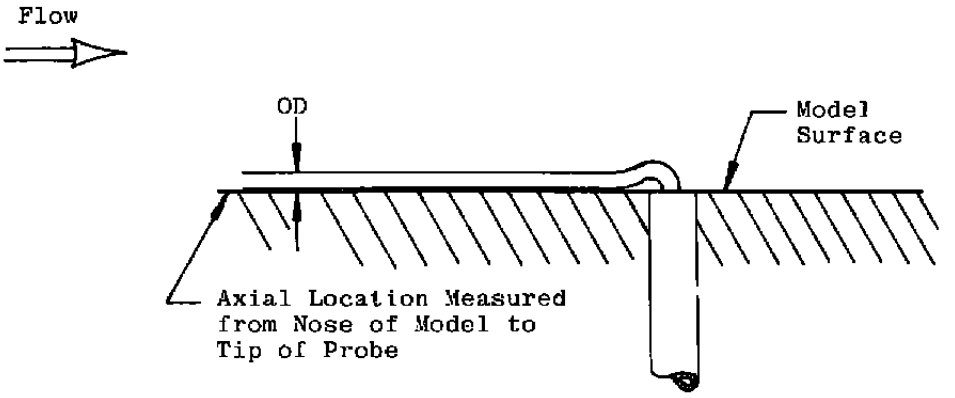

Preston Tube No.	x Location, in.	x/L	Outside Diam, in.	θ, deg
1	26.049	0.200	0.014	5
2	39.338	0.302	0.014	275
3	52.028	0.400	0.014	95
4	60.231	0.463	0.022	265
5	84.582	0.650	0.022	355
6	91.348	0.702	0.022	265
7	103.743	0.798	0.032	95
8	117.207	0.901	0.032	355
9	125.209	0.963	0.032	275

Figure 8. Preston tube installation on EBOR model.

2.3.3 Boundary-Layer Rakes

Four total pressure boundary-layer rakes were mounted normal to the surface on the EBOR model. Each rake consisted of eleven 0.032-in.-OD stainless-steel tubes protruding 0.5-in. from the leading edge of a stainless-steel strut. The leading edge of the strut was a 30-deg wedge. Each strut was 0.125 in. thick with a chord of 0.813 in. A sketch of a typical rake and the axial locations and tube spacing of the four boundary-layer rakes is presented in Fig. 9. The locations and rake dimensions were selected based on calculations of boundary-layer thickness distribution and velocity profiles performed using the SWIM computer code described in Ref. 10. Measurement locations were selected so round tubing of practical size could be used to measure several points in the logarithmic region of the velocity profile over the expected range of operating conditions.

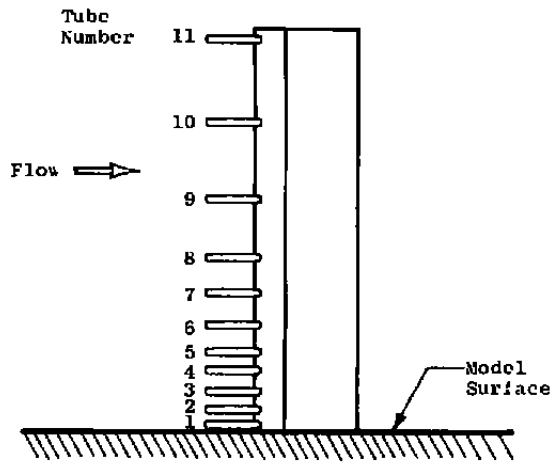

Rake No.	1	2	3	4
Model Station, in.	94.731	106.048	113.828	121.597
Radial Location, deg	247.5	22.5	112.5	337.5
Tube 1	0.018*	0.020	0.020	0.020
2	0.088	0.090	0.085	0.185
3	0.158	0.170	0.165	0.370
4	0.238	0.245	0.245	0.580
5	0.333	0.340	0.350	0.815
6	0.458	0.470	0.465	1.070
7	0.603	0.620	0.615	1.410
8	0.778	0.790	0.795	1.845
9	1.053	1.065	1.070	2.470
10	1.408	1.425	1.420	3.260
11	1.758	1.765	1.765	4.040

*Distance from model surface to tube center in inches.

Figure 9. Boundary-layer rake installation on EBOR model.

3.0 PROCEDURES

3.1 CALIBRATION

3.1.1 Experiments in the ART (Phase I)

The embedded-wire gages received a temperature-resistance calibration prior to installation in the ART. The purpose of the temperature-resistance calibration is to enable the gage to be used as a temperature measuring device for determining the temperature rise of the gage during operation. The gages were calibrated by placing them in an oven, subjecting them to a range of temperatures, and measuring the gage resistance, which is a linear function temperature. The coefficients of the calibration curve were determined by a linear least-squares regression fit of the data. A typical temperature-resistance calibration is presented in Fig. 10.

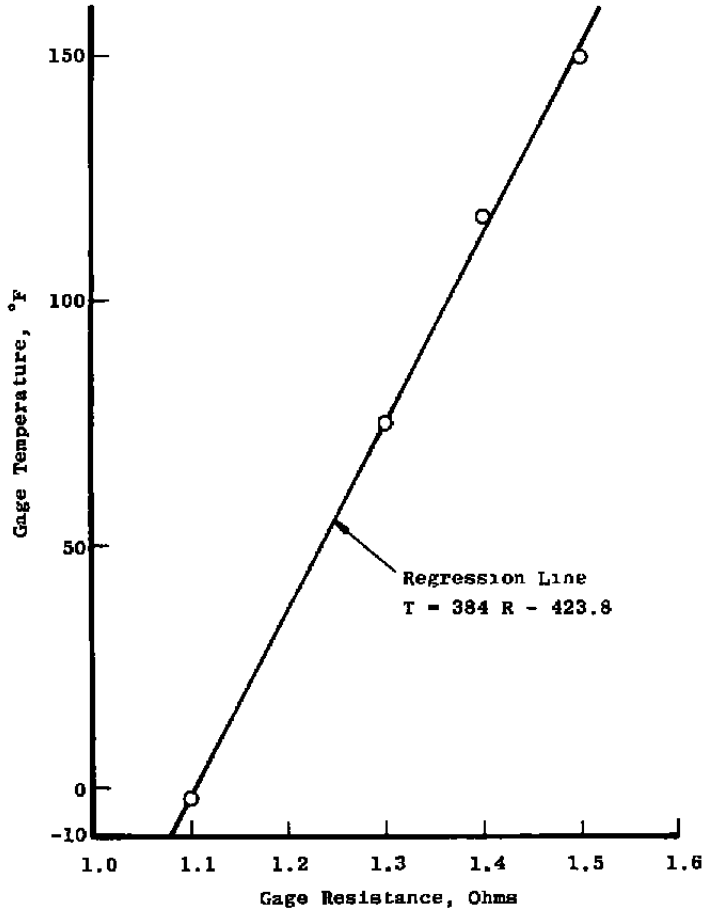

Figure 10. Typical calibration curve for an embedded-wire gage.

After the temperature-resistance calibration procedure, the embedded-wire gage was installed at the axial location indicated in Fig. 2. Before each run, the gage temperature-resistance calibration was checked and the tunnel pressure system calibrated. The temperature-resistance calibration was checked by comparing the temperature inferred from measurements of the gage resistance with the temperature measured by the copper-constantan thermocouple mounted on the tunnel wall. A range of adiabatic wall temperatures was obtained by varying Mach number at a constant total temperature. Shifts in the temperature-resistance curve were recorded during experiments in the ART; however, repeat gage calibrations indicated that the slope of the curves remained constant. Therefore, it was possible to correct the coefficients of the calibration curve before each testing period.

The embedded-wire gage was calibrated over a range of shear stress values using a Preston tube as a calibration standard. The output of the embedded-wire gage is the power loss per unit temperature rise, and is proportional to the cube root of the density at the wall times the wall shear stress divided by the square of the dynamic molecular viscosity at the wall. The calibration coefficients were determined by a standard least-squares linear regression fit of the calibration data. A typical set of calibration data is presented in Fig. 11.

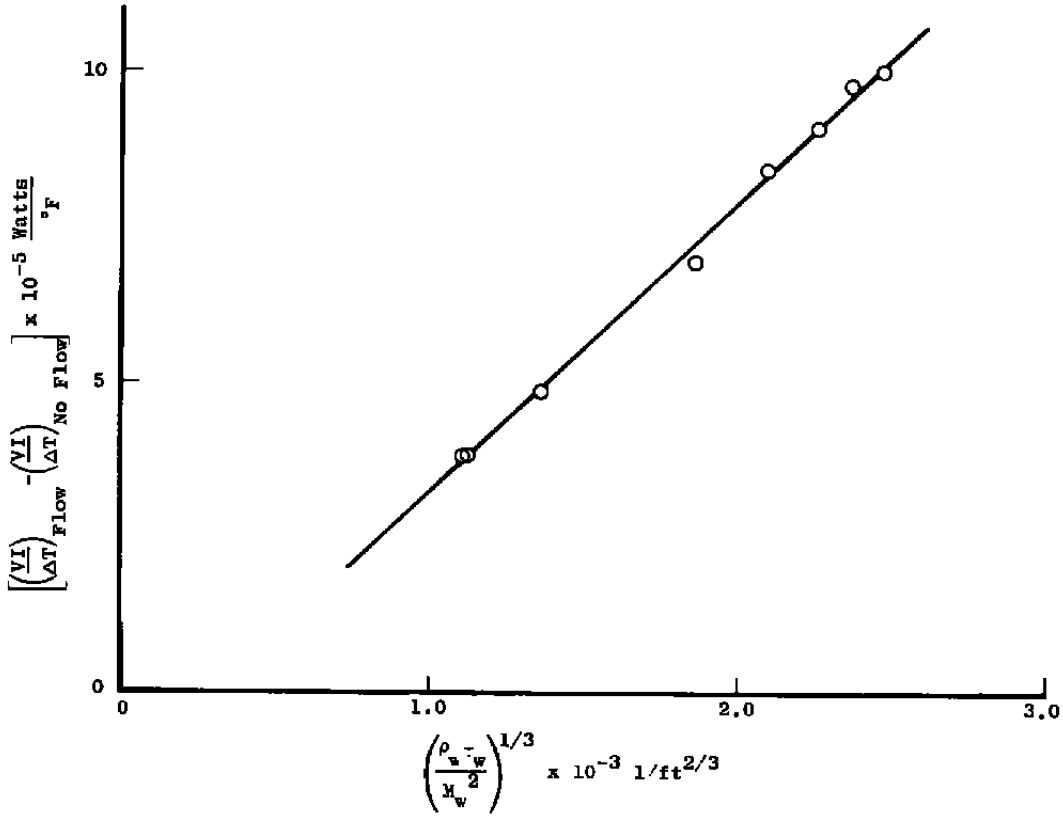

Figure 11. Typical embedded-wire shear stress calibration.

3.1.2 Experiments in Tunnel 16T (Phase II)

The embedded-wire gages were calibrated in groups of 10 in the ART by the method described in Section 3.1.1 and installed in the EBOR model at the axial locations shown in Table 1. Subsequent analysis of the Tunnel 16T test data indicated that the calibration constants were affected by the move from the ART to the EBOR model. The installation process with the EBOR model apparently caused changes in gage stress which produced shifts in the temperature-resistance relationships for each gage. Simple corrections to the calibration constants were not possible because the slopes of the curves had changed. A new set of calibration constants was determined from the Preston tube and boundary-layer rake

measurements taken at a free-stream Mach number of 0.6 and unit Reynolds numbers of 1.5, 2.25, and 3.35 x 10^6 per ft. Calculations using the SWIM computer code (Ref. 10) were used to obtain data between measurement locations and regions where measurements were not available. The set of calibration constants determined in this manner was used to reduce all embedded-wire data measured on the EBOR model.

The six-component balance used in the EBOR model was calibrated from 0 to 400 lb in the axial direction. Greater accuracy than normal was achieved by calibrating only one component of the balance instead of developing a calibration for all six components.

3.2 DATA ACQUISITION

3.2.1 Experiments in the ART (Phase I)

The ART was operated at Mach numbers from 0.1 to 0.8. At each Mach number, the wall temperature was monitored until adiabatic wall conditions were reached, as indicated by a zero change in wall temperature with time. The cold resistance of the embedded-wire gage was recorded at the adiabatic wall condition. The potentiometer was then adjusted to drive the gage to a predetermined resistance value which is related to the desired temperature rise of the gage. The heated resistance, the voltage across the gage, and the current through the gage were recorded. Preston tube pressure, wall static pressure, wall temperature, tunnel total temperature, tunnel total pressure, and free-stream Mach number were also recorded.

3.2.2 Experiments in Tunnel 16T (Phase II)

Data on the EBOR model were acquired in two modes in Tunnel 16T. The first mode was performed to obtain Preston tube and boundary-layer rake data. The test matrix is presented in Table 2. Total temperature was varied as a function of Mach number to maintain a constant adiabatic wall temperature throughout the test. This procedure shortened test time by eliminating the need to wait for the model to reach thermal equilibrium between each condition in the test matrix. Once test conditions were established, steady-state data were recorded by the facility computer.

For the second mode, the Preston tubes and boundary-layer rakes were removed and the test matrix was repeated to obtain balance, pressure, and embedded-wire data. The embedded-wire gages were operated as described in Section 3.2.1, and the facility computer recorded steady-state data at each test condition. Repeat points were obtained at a free-stream Mach number of 0.6 and a unit Reynolds number of 3.35 x 10^6 per ft.

Table 2. Test Matrix for EBOR Model

Free-Stream Mach Number M_∞	Free-Stream Unit Reynolds Number, $Re_\infty \times 10^{-6}$/ft	Total Temperature °R	With Rakes and Preston Tubes	Without Rakes and Preston Tubes	
				Dry	Wet
0.6	1.5	565	x	x	
0.6	2.25	565	x	x	
0.6	3.35	565	x	x	x
0.6	3.35	570			x
0.6	3.35	580			x
0.6	5.0	585	x	x	
0.9	3.35	570	x	x	x
1.2	3.35	575	x	x	x
1.5	3.35	580	x	x	x

3.3 DATA REDUCTION

3.3.1 Experiments in the ART (Phase I)

The wall shear stress was determined from the embedded-wire measurements by applying the calibration law presented by Murthy and Rose (Ref. 5),

$$\frac{\rho_w \tau_w (\lambda \ell)^2 \, Pr}{\mu_w^2} = 1.9 \, Nu^3 - 0.2778 \frac{\rho_w (\lambda \ell)^3 \, Pr}{\mu_w^2} \frac{dp}{dx} \frac{1}{Nu} \tag{1}$$

For a single gage with a small streamwise dimension operated in air, Eq. (1) reduces to

$$\frac{\rho_w \tau_w}{\mu_w^2} \propto Nu^3 \tag{2}$$

where the Nusselt number is proportional to the gage output, (Ref. 5)

$$Nu = \frac{q - q_o}{sk \, \Delta T} = \frac{(VI)_{flow}}{\Delta T} - \frac{(VI)_{no\ flow}}{\Delta T} \tag{3}$$

when Eqs. (1) and (3) are combined, the power loss from the gage per degree of temperature rise can be expressed as a function of wall shear stress and fluid properties at the wall

$$\frac{VI}{\Delta T} = \frac{(VI)_{flow}}{\Delta T} - \frac{(VI)_{no\ flow}}{\Delta T} = A \left(\frac{\rho_w \tau_w}{\mu_w^2} \right)^{1/3} - B \tag{4}$$

The constants A and B were determined by the calibration procedure described in Section 3.1.1. The value ΔT is proportional to ΔR; therefore, the quantity ΔR was used throughout to simplity calculations. With $\Delta T \propto \Delta R$, Eq. (4) becomes

$$\frac{VI}{\Delta R} = A\left(\frac{\rho_w \tau_w}{\mu_w^2}\right)^{1/3} + B \tag{5}$$

The constant of proportionality between ΔT and ΔR is incorporated into the constants A and B during calibration. With the constants A and B known, the wall shear stress was calculated by solving Eq. (5) for τ_w

$$\tau_w = \left[\frac{1}{A}\left(\frac{VI}{\Delta R} - B\right)\right]^3 \tag{6}$$

The skin-friction coefficient was calculated by dividing the wall shear stress by the free-stream dynamic pressure

$$C_f = \frac{\tau_w}{q_\infty} \tag{7}$$

The Preston tube data reduction technique developed by Allen (Ref. 13) was used to determine the corresponding skin-friction coefficient.

3.3.2 Experiments in Tunnel 16T (Phase II)

Local skin-friction coefficients were measured on the EBOR model using Preston tubes, boundary-layer rakes, and embedded-wire gages. The C_f values were computed from the embedded-wire gage and Preston tube measurements by the methods presented in Section 3.3.1. The boundary-layer rake measurements were used in a program developed by Whitfield (Ref. 14) to calculate the velocity profile, displacement thickness, momentum thickness, and shape factor. The local skin-friction coefficient associated with the measured profile was found by fitting the data to the compressible law of the wall as formulated by Fenter and Stalmach (Ref. 15).

Total skin-friction drag was determined by numerically integrating the individual embedded-wire values over the model surface assuming that the body and flow were perfectly axisymmetric. The integration of skin-friction drag force can be expressed as

$$F = \sum_{i=1}^{N+1} \frac{f_i + f_{i-1}}{2} A_i \cos\theta_i$$

where

$$\cos\theta_i = \frac{x_i - x_{i-1}}{\left[\left(r_i - r_{i-1}\right)^2 + \left(x_i - x_{i-1}\right)\right]^{1/2}} \tag{8}$$

$$f_o = 0 \qquad x_o = 0$$

$$f_{N+1} = f_N \qquad r_o = 0$$

The total skin-friction drag coefficient is

$$C_{f_T} = \frac{F}{q_\infty S} \tag{9}$$

For comparison with the embedded-wire data, the total skin-friction drag coefficient was also estimated from balance and pressure data by subtracting the numerically integrated pressure force coefficient from the balance measured total drag coefficient. The pressure integrated drag coefficient is based on the maximum cross-sectional area of the model and determined by

$$C_{DP} = C_{DF} - C_{DA} - C_{CAV} \tag{10}$$

where C_{DF} is forebody pressure drag coefficient, C_{DA} is the afterbody pressure drag coefficient, and C_{CAV} is the model cavity force coefficient. The total skin-friction drag coefficient, C_{f_B}, was calculated as

$$C_{f_B} = C_D - C_{DP} \tag{11}$$

where C_D is the balance measured drag coefficient.

3.4 DATA UNCERTAINTY

The uncertainties (combinations of systematic and random errors) of the basic tunnel parameters, shown in Figs. 12 and 13 for the ART and Tunnel 16T, respectively, were estimated from repeat calibration of the instrumentation and from the repeatability and uniformity of the test section flow during tunnel calibration. Uncertainties in the instrumentation systems were estimated from repeat calibration of the systems against secondary standards whose uncertainties are traceable to the National Bureau of Standards calibration equipment. The instrument uncertainties, for a 95-percent confidence level, are combined using the Taylor series method of error propagation described in Ref. 16 to determine the uncertainties of the reduced parameters shown in Table 3.

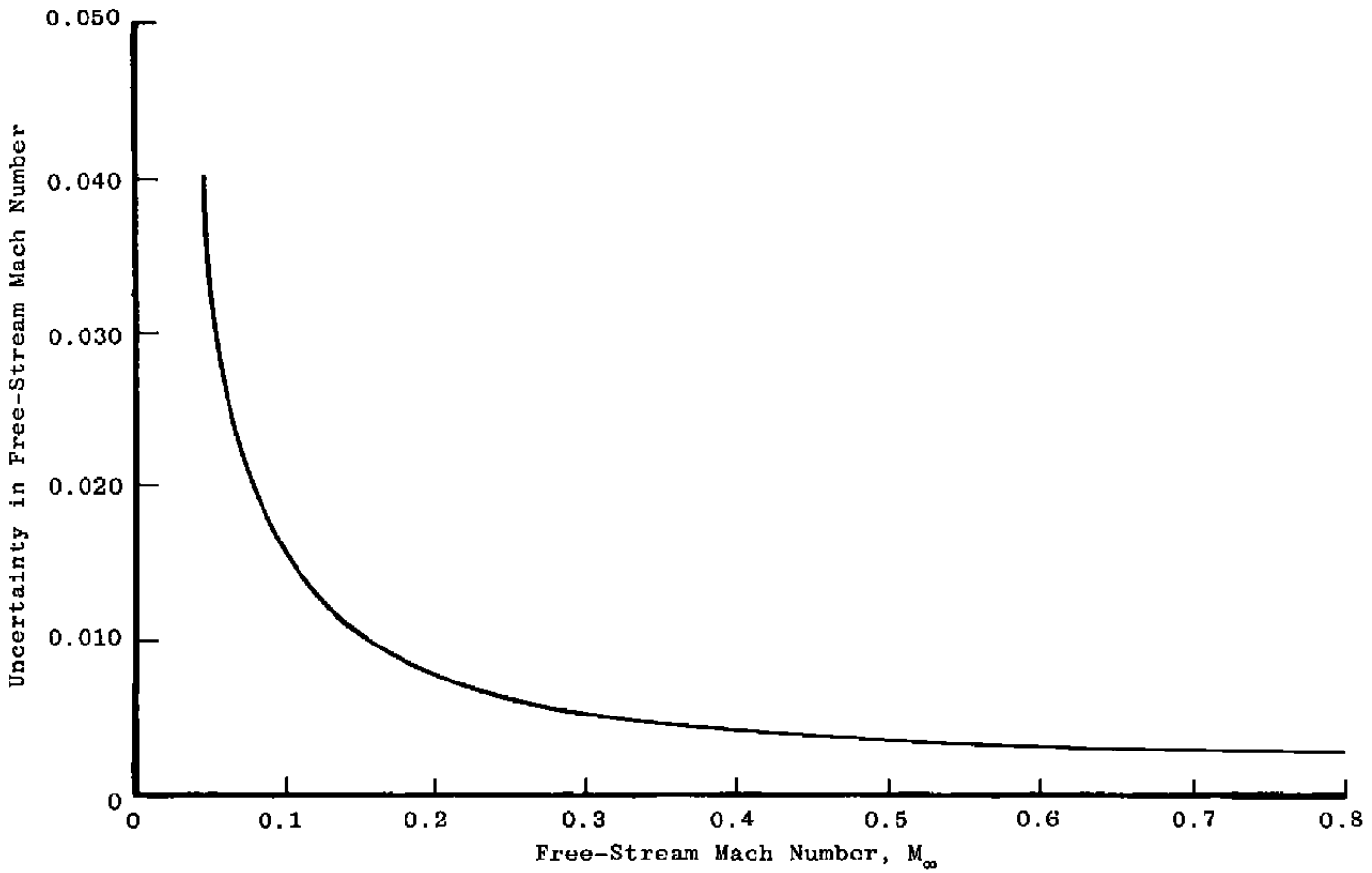

Figure 12. Estimate of the uncertainty in the free-stream Mach number for the ART.

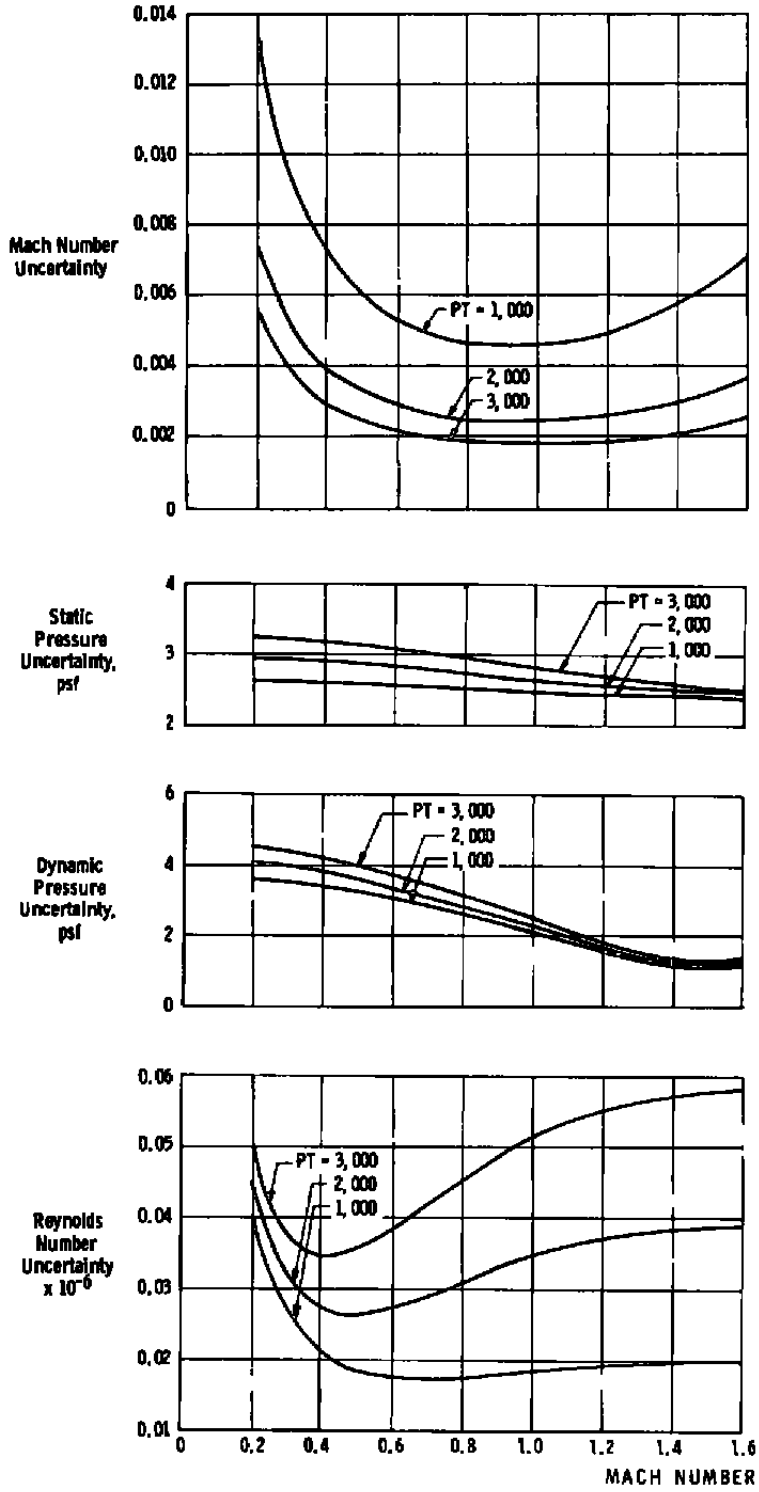

Figure 13. Estimated uncertainties in wind tunnel parameters for Tunnel 16T.

Table 3. Measurement Uncertainties

Parameter	Uncertainty			
	$M_\infty = 0.6$ $T_T = 565°R$	$M_\infty = 0.9$ $T_T = 570°R$	$M_\infty = 1.2$ $T_T = 575°R$	$M_\infty = 1.5$ $T_T = 580°R$
P, psf	±4.800	±4.500	±4.400	±4.400
C_p	±0.0063	±0.0037	±0.0027	±0.0022
C_{DP}	±0.0033	±0.0017	±0.0010	±0.0006
C_D	±0.0019	±0.0013	±0.0013	±0.0011
C_{f_B}	±0.0038	±0.0021	±0.0016	±0.0013
C_f	±0.0004	±0.0005	±0.0003	±0.0003
C_{f_T}	±0.0069	±0.0073	±0.0060	±0.0058

Note: Data uncertainty values are presented at a free-stream unit Reynolds number of 3.35×10^6/ft.

4.0 RESULTS

4.1 EXPERIMENTS IN THE ART (PHASE I)

The temperature-resistance calibration presented in Fig. 10 is typical for the embedded-wire gages tested in the ART. The calibration is linear over the range of operating temperatures expected in the ART and Tunnel 16T; however, repeated experiments revealed that shifts in the calibration constants for a particular gage can occur between periods of operation. An attempt was made to determine the cause of the calibration shift, but no apparent explanation was discovered. The nature of the calibration shift observed in the ART provided a simple method for correcting the calibration coefficients. The data presented in Fig. 14 are repeat calibrations of a single gage. The data sets are displaced, but the $\partial T/\partial R$ remains the same. Therefore, only the zero intercept of the calibration curve must be corrected. This can be accomplished by measuring the gage resistance at a known value of temperature and calculating a new zero intercept using the calibration slope

$$b = T - aR \tag{12}$$

Because the $\partial T/\partial R$ remained constant, the gage can be used to measure differences in temperature without any correction to the zero intercept

$$\Delta T = a\,\Delta R \tag{13}$$

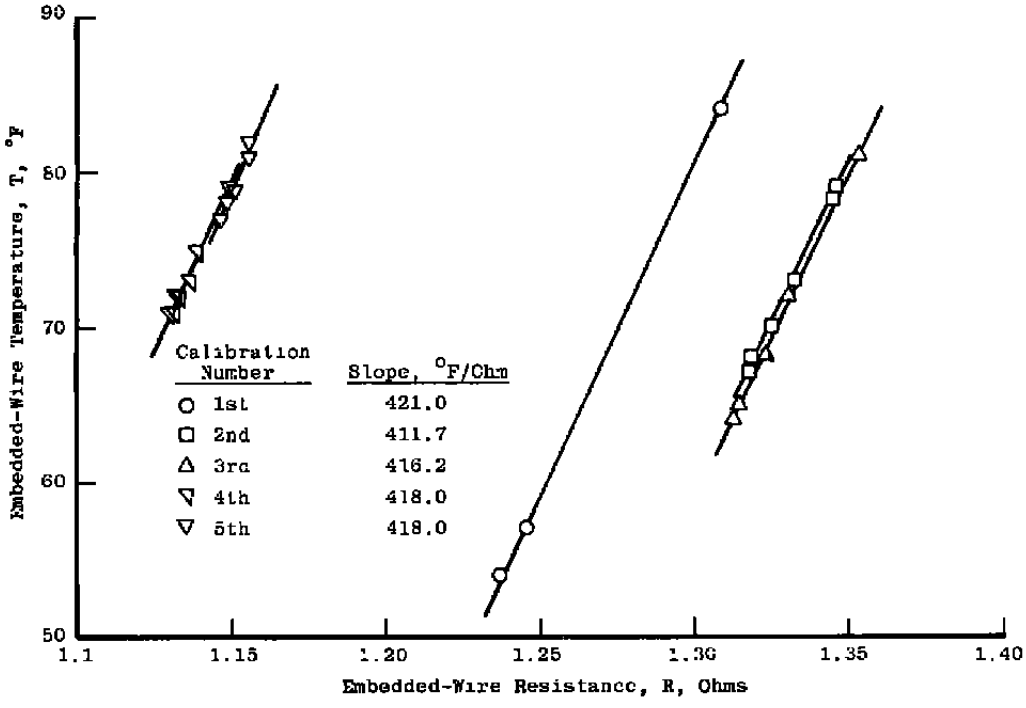

Figure 14. Repeat temperature-resistance calibration of an embedded-wire gage.

The gage calibration presented in Fig. 11 was produced by plotting the power per unit temperature rise versus the cube root of the density times the wall shear stress divided by the square of the viscosity $(\varrho_w \tau_w / \mu_w^2)^{1/3}$. The density and viscosity are evaluated at the wall temperature and pressure. The wall shear stress was determined by Preston tube measurements. In Fig. 15, C_f computed from Preston tube measurements is compared with boundary-layer profile measurements performed previously with the same test apparatus by Benek (Ref. 9). The agreement between the two techniques is very good, and the Preston tube method was used to determine C_f, eliminating the time-consuming task of measuring pressure profiles at each calibration point.

Rubesin, et al. (Ref. 4) and Murthy and Rose (Ref. 5) report that a two-point calibration is sufficient using the wind-off value ($\tau_w = 0$) as one of the calibration points. This calibration procedure assumes that the calibration curve passes through the origin in Fig. 11. This was not always true for the embedded-wire gages tested in the ART. To reduce the uncertainty in the calibration coefficients, a multipoint calibration was performed, and the coefficients were determined by a linear regression fit of the data.

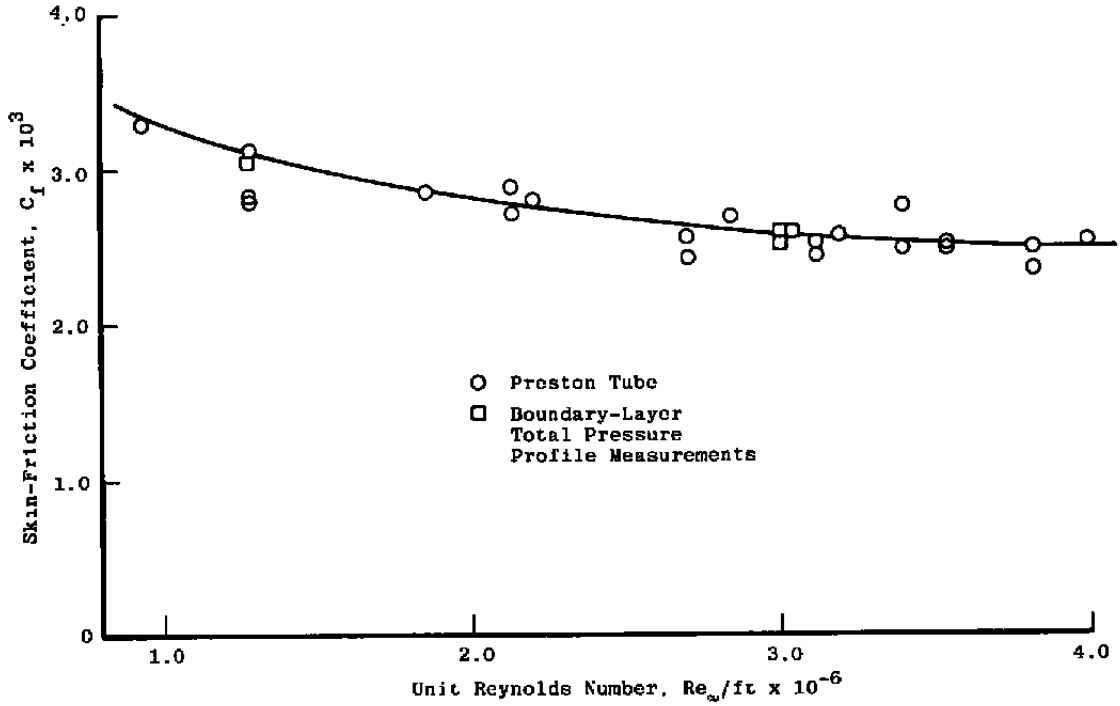

Figure 15. Comparison of skin-friction coefficient from Preston tube and boundary-layer profile measurements.

Bellhouse and Schultz (Ref. 3) reported that the sensitivity of the heated-element gage was dependent on the amount of temperature rise, ΔT, selected for operation. Results obtained in the ART support their findings. Calibration curves generated at different values of ΔT are presented in Fig. 16. As the value of ΔT is increased, the slope of the calibration curve decreases, a condition produced by heat conduction in the subtrate material, which changes the effective length of the gage. Therefore, the gage must be operated at the same value of ΔT used during calibration. The repeatability of operating an embedded-wire gage at the same value of ΔT is presented in Figs. 17 and 18. In Fig. 17, the gage output is plotted versus the Preston tube determined shear stress parameter for two operation periods. The two sets of data are essentially the same. In Fig. 18, the skin-friction coefficients determined from repeat embedded-wire data agree with those from the Preston tube measurements to within 10 percent. Between the two run periods, an unexplained shift occurred in the gage temperature-resistance calibration as shown in Fig. 19. By adjusting the calibration coefficients and operating the gage at a constant value of ΔT, the skin-friction determination was unaffected.

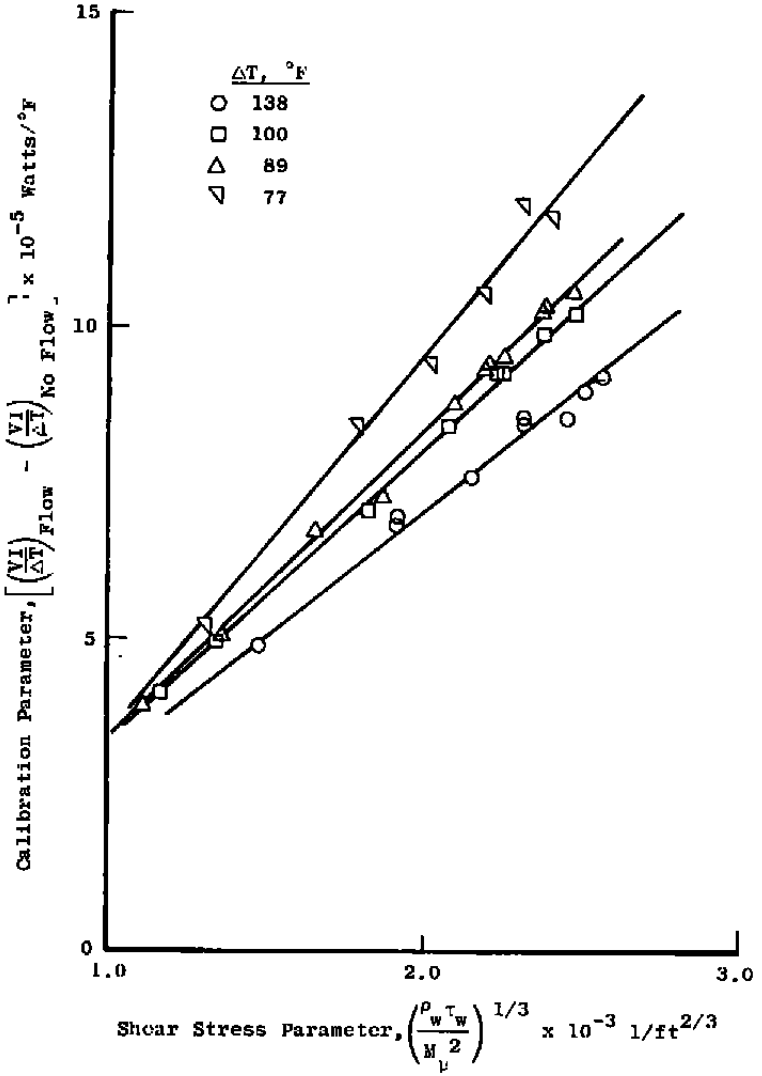

Figure 16. Effect of operating temperature on the embedded-wire calibration.

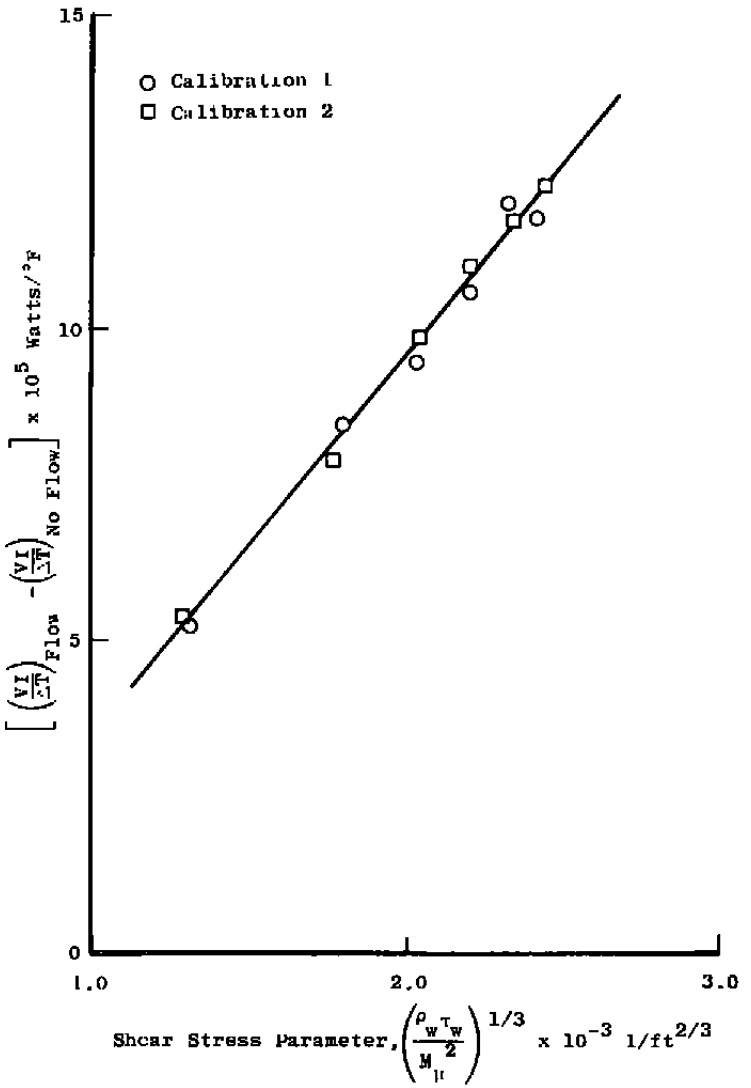

Figure 17. Calibration repeatability.

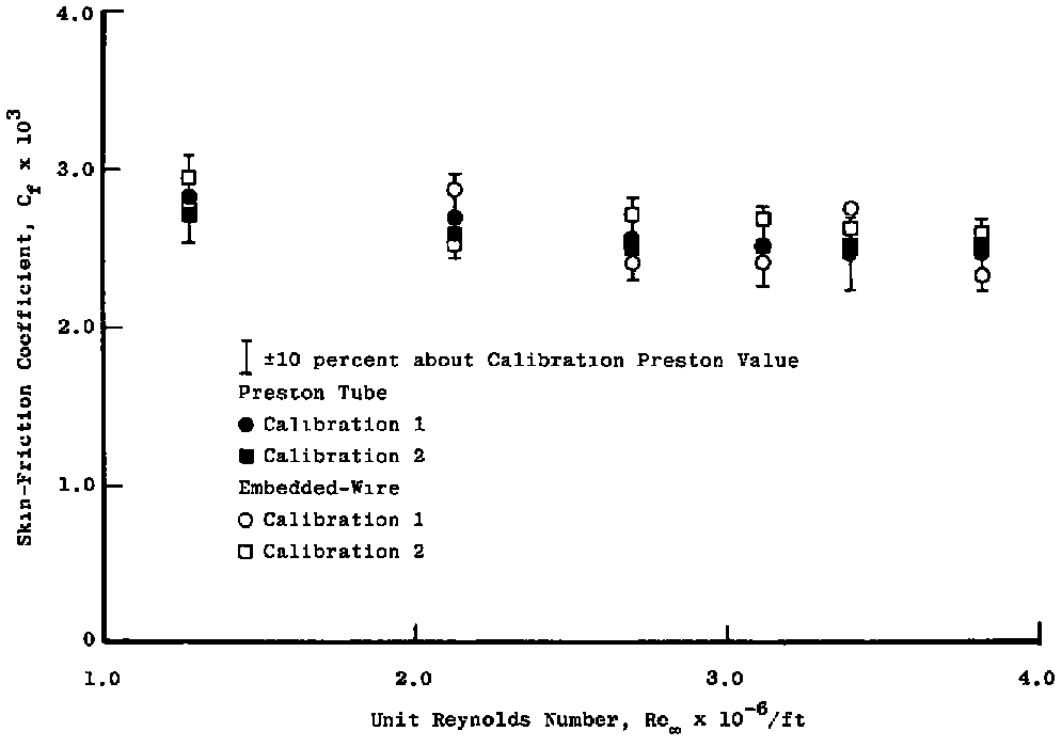

Figure 18. Comparision of repeated measurements of skin-friction coefficient in the ART.

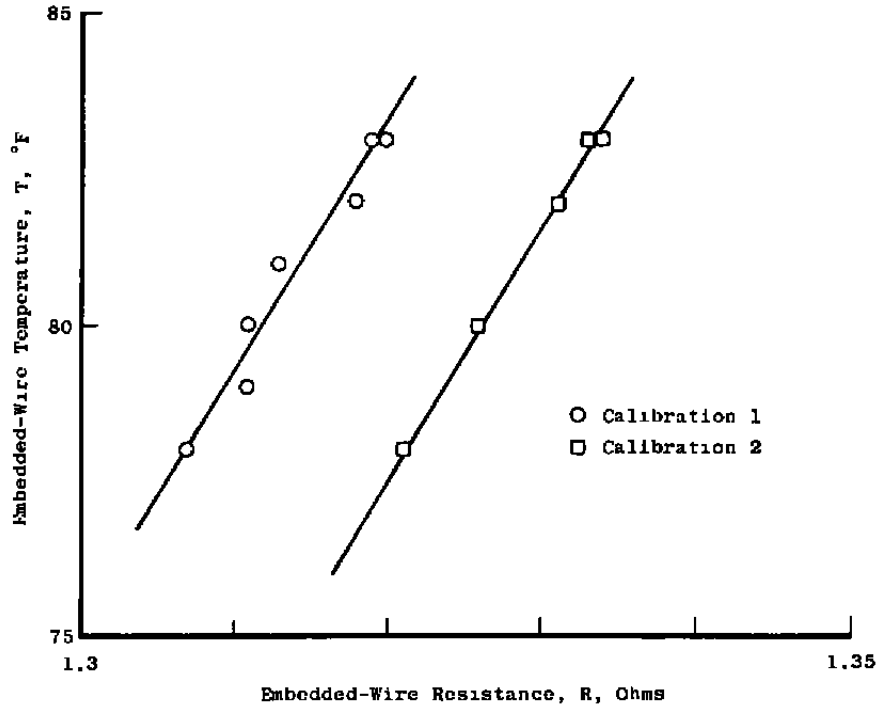

Figure 19. Comparison of temperature-resistance curves for repeat calibration of a single embedded-wire gage.

4.2 EXPERIMENTS IN TUNNEL 16T (PHASE II)

Measurements of local skin-friction coefficient distributions on the EBOR model are presented in Fig. 20. At subsonic Mach numbers, the agreement between Preston tube and boundary-layer rake measurements and SWIM calculations is good at all values of unit Reynolds number. The embedded-wire gages also agree well except at a Mach number of 0.6 and a unit Reynolds number of 5 x 10^6 per ft (Fig. 20d). At this test condition, the embedded-wire gages indicated lower values of local skin friction than the other techniques. However, the data are still within 10-percent agreement.

At supersonic conditions (Figs. 20f and g) the various methods agree well on the forebody of the model, but not on the afterbody, particularly on the boattail. At these test conditions the presence of severe axial and radial pressure gradients in the flow field and a shock wave on the boattail violates assumptions used in relating the Preston tube and boundary-layer rake data to skin friction. Also, the surface pressures measured on the boattail at the supersonic Mach numbers were close to the pressure values at which Murthy and Rose (Ref. 5) report a reduction in the conduction heat loss from the embedded-wire gages. This reduction decreases the output from the embedded-wire gage for a given value of local shear stress, and the value of the local skin-friction coefficient implied by the gage reading is lower than the actual value. The scatter in the embedded-wire data is a combination of the uncertainty in the measurements and not being at exactly adiabatic conditions at the time of data acquisition. This problem is related to the length of time required to set up the gages at each test condition. Surface temperatures on the model are recorded before adjusting the gages, and those temperatures were used to calculate local density, viscosity, and the temperature setting for each gage. If the model temperature changes during the setup period, the gages will not be adjusted properly when data are taken. During the experiment, the total temperature of the tunnel was adjusted to maintain a constant adiabatic wall temperature on the model. However, the model temperature increased 2°F as unit Reynolds number was increased. In Fig. 21, a comparison of repeated embedded-wire gage measurements is presented. Before the test condition was repeated, the model was 0.5°F higher than the adiabatic temperature during acquisition of the primary data. The fact that the repeated data are higher than the primary data is indicative of the model temperature decrease during gage adjustment. This problem can be corrected by assuring that the adiabatic wall condition has been reached, by shortening setup time, or by monitoring the temperature of each gage and correcting for any changes that occur during adjustment of the gages.

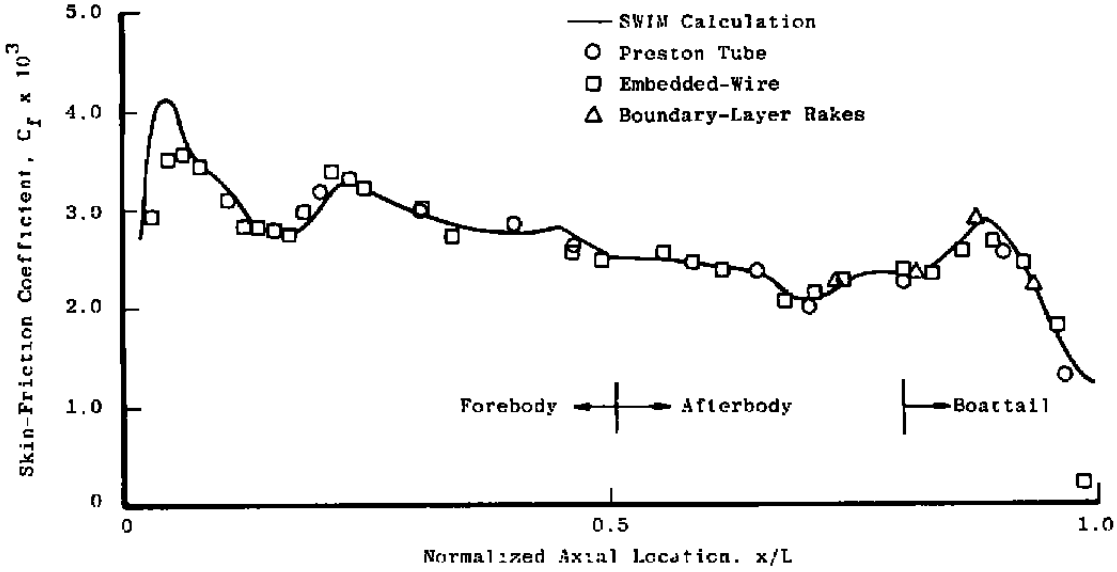

a. $M_\infty = 0.6$ $Re_\infty/ft = 1.5 \times 10^6$

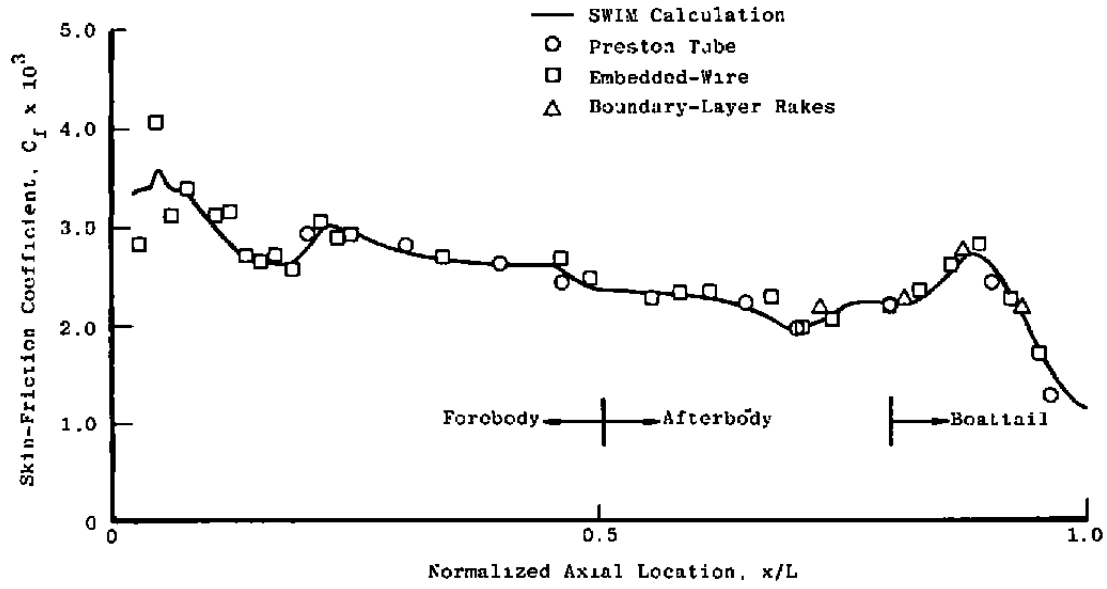

b. $M_\infty = 0.6$ $Re_\infty/ft = 2.25 \times 10^6$

Figure 20. Measured and calculated local skin friction on the EBOR model.

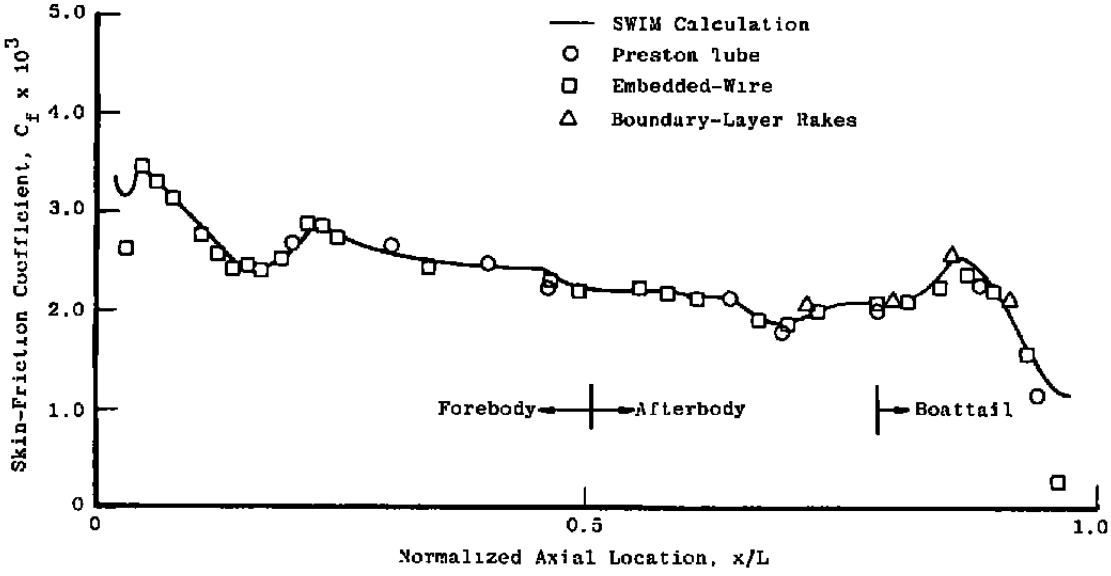

c. $M_\infty = 0.6$ $Re_\infty/ft = 3.35 \times 10^6$

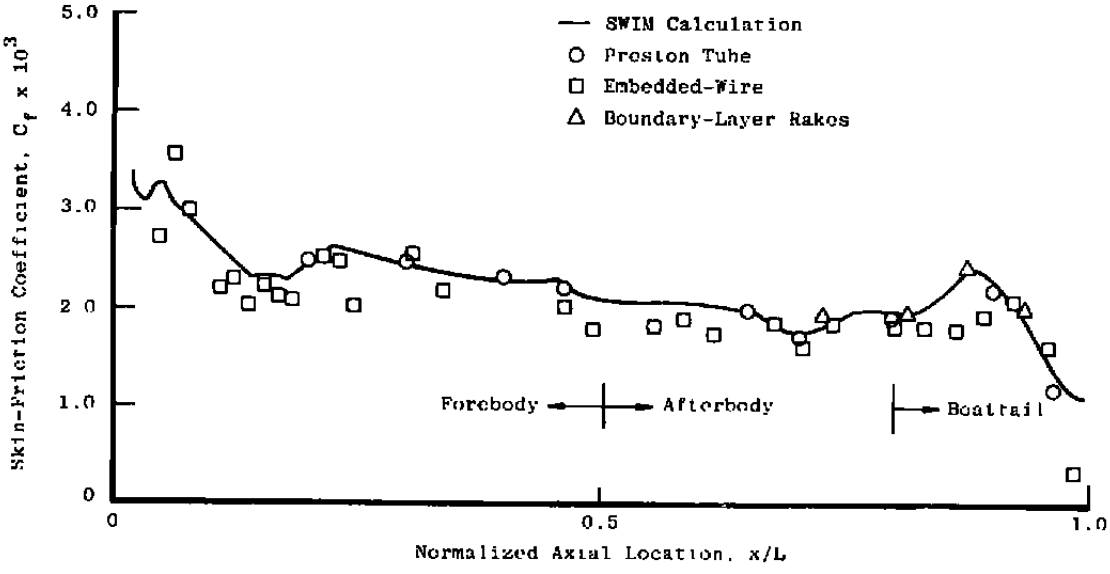

d. $M_\infty = 0.6$ $Re_\infty/ft = 5 \times 10^6$

Figure 20. Continued.

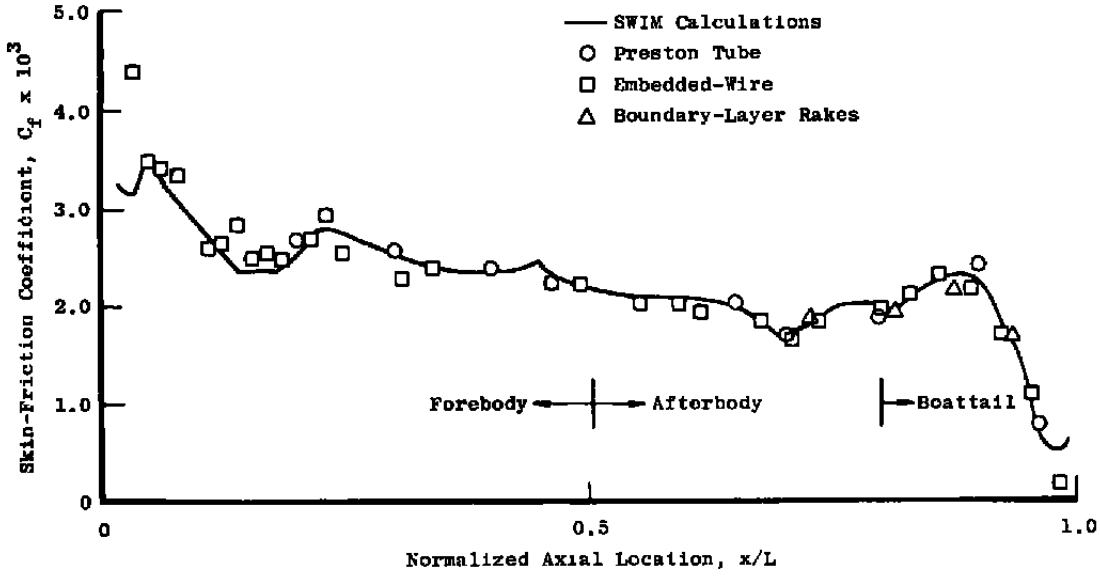

e. $M_\infty = 0.9$ $Re_\infty/ft = 3.35 \times 10^6$

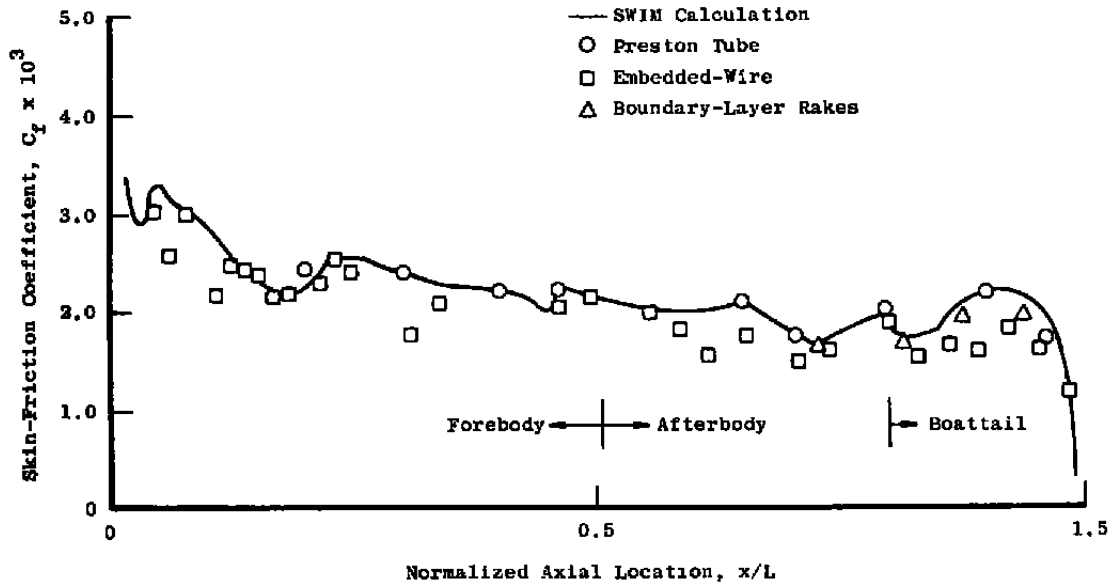

f. $M_\infty = 1.2$ $Re_\infty/ft = 3.35 \times 10^6$

Figure 20. Continued.

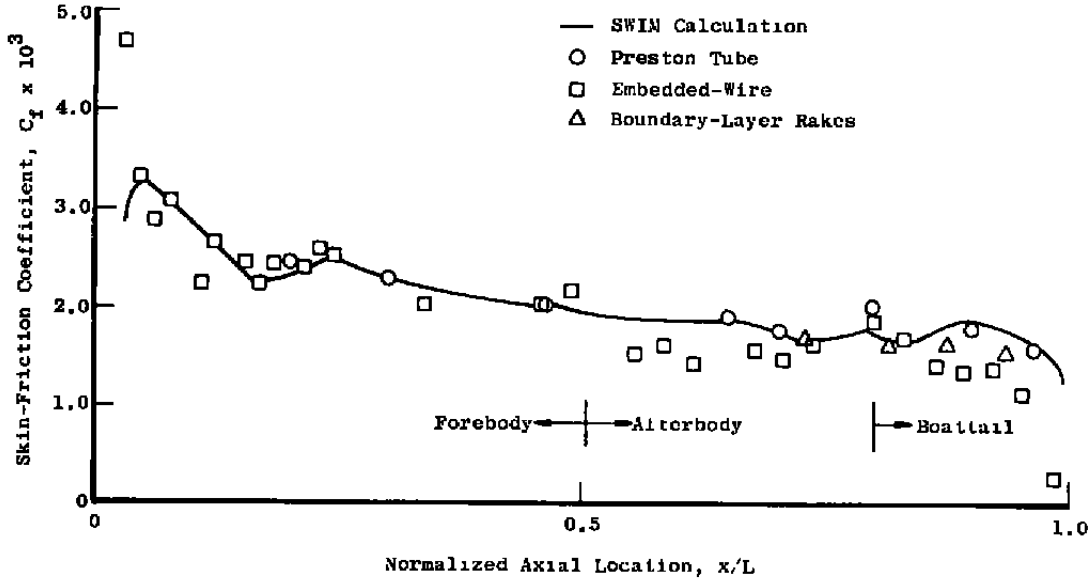

g. M_∞ =1.5 Re_∞/ft = 3.35 x 10^6
Figure 20. Concluded.

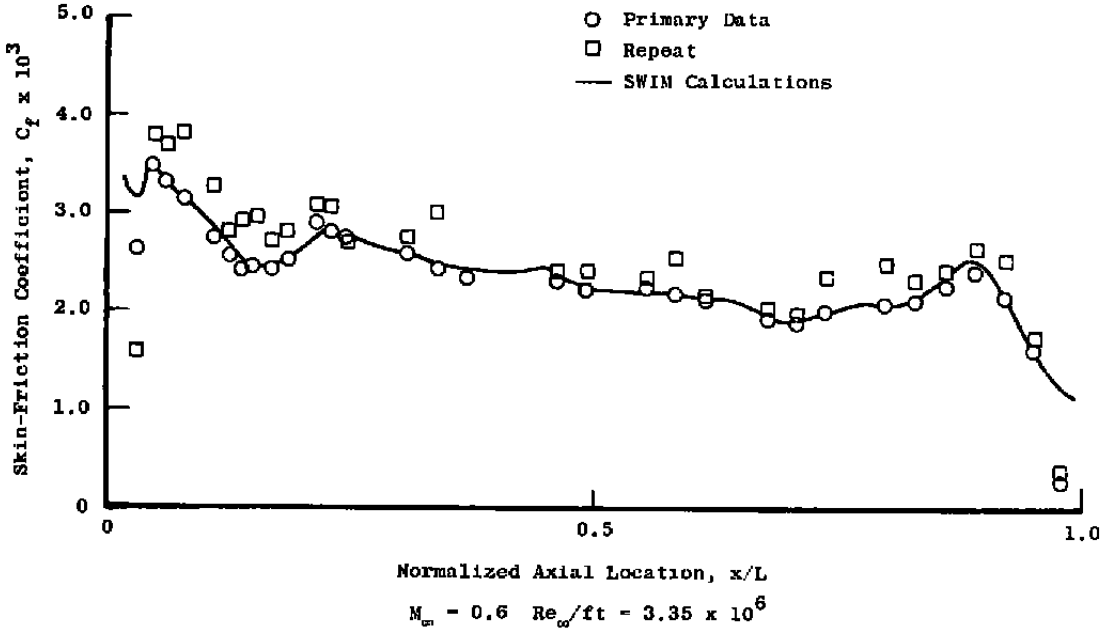

Figure 21. Repeated embedded-wire measurements.

Comparisons of measured and calculated total skin-friction drag coefficients are presented in Figs. 22 and 23 for constant Mach number and constant unit Reynolds number, respectively. The agreement between embedded-wire gage and balance minus pressure measured skin-friction drag is good at all test conditions. Agreement with SWIM calculations is also good except at the higher Mach numbers. This disagreement is caused by the higher values of skin friction calculated on the boattail by the SWIM code at the supersonic conditions (see Figs. 21f and g).

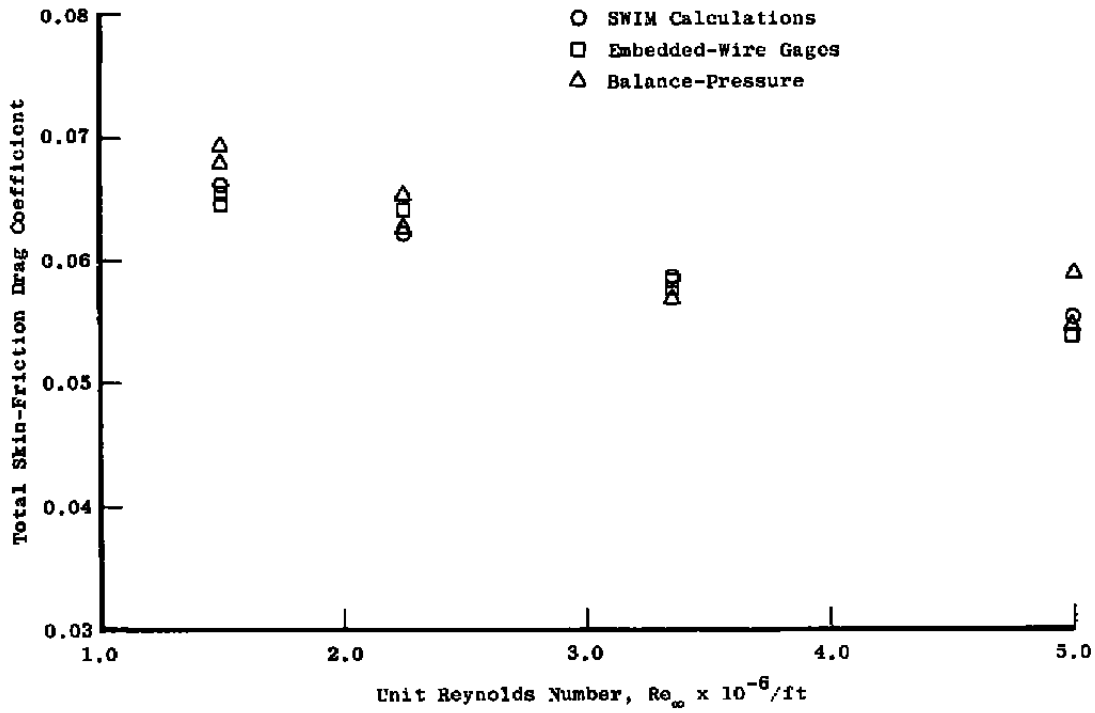

Figure 22. Total skin-friction drag coefficients at Mach number 0.6.

In Fig. 24, a parameter proportional to skin-friction coefficient is plotted versus Reynolds number for the first five gages on the model. The parameter was determined from the relation

$$\left(\frac{\rho_w \tau_w}{\mu_w^2}\right)^{1/3} \propto \frac{VI}{\Delta R} \tag{14}$$

By solving for τ_w and dividing both sides by the free-stream dynamic pressure, the skin-friction parameter was defined as

$$C_{f_u} = \frac{\tau_w}{q_\infty} \propto \frac{\mu_w^2}{\rho_w q_\infty}\left(\frac{VI}{\Delta R}\right)^3 \tag{15}$$

C_{f_u} from gage 2 decreases with increasing Reynolds number and then increases at the highest Reynolds number. This behavior would be expected for a gage initially in a laminar boundary layer and entering transition. C_{f_u} for gage 3 increases with increasing Reynolds number and then decreases. This behavior would be expected for a gage initially in the boundary-layer transition region with the flow becoming fully turbulent. Since the gages are aligned in the axial direction, gage 3 is in transition at a lower Reynolds number than gage 2

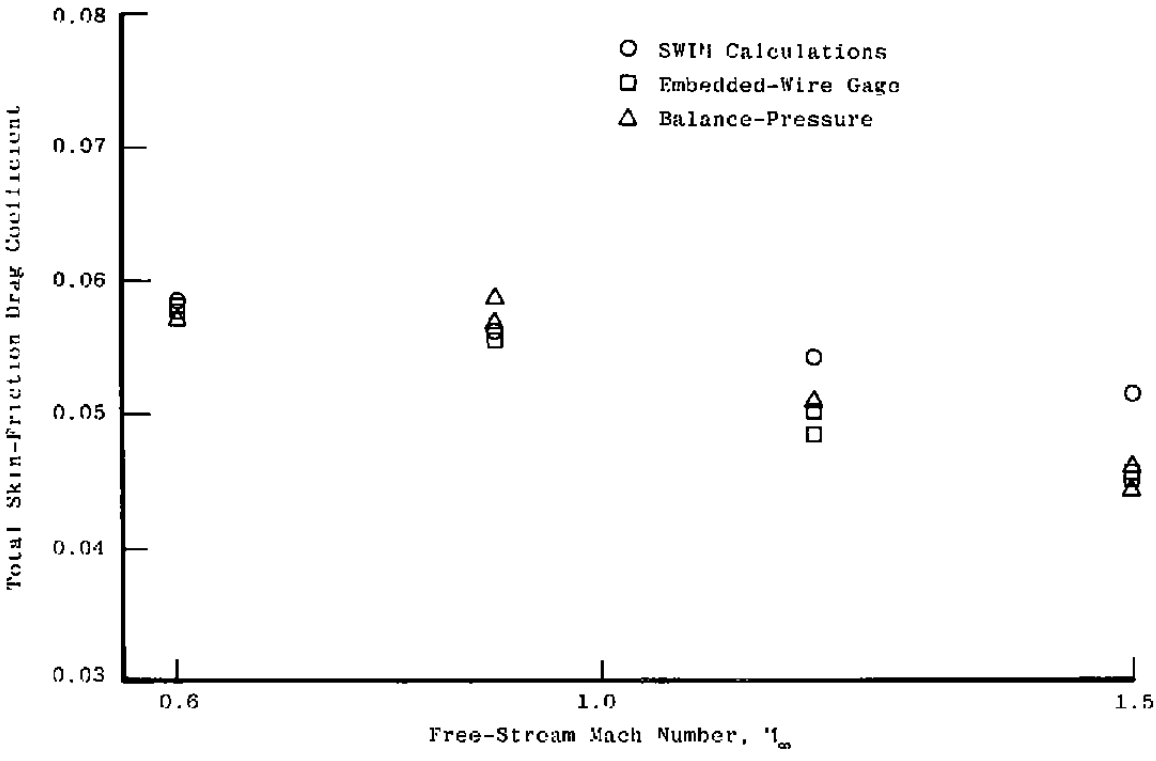

Figure 23. Total skin-friction drag coefficients at unit Reynolds number 3.35 x 10^6/ft.

because the boundary layer is tripped by gage 2. C_{f_u} variation for the remaining gages decreased with increasing Reynolds number, indicating that these gages are in fully turbulent flow. Since calibration is not necessary to detect transition, the gages possibly can be contoured to model surface to avoid their tripping the boundary layer. However, it would appear from the data in Fig. 24 that a single gage would not give sufficient information about the state of the boundary layer unless the gage can be subjected to at least two different flow regimes over the range of test conditions.

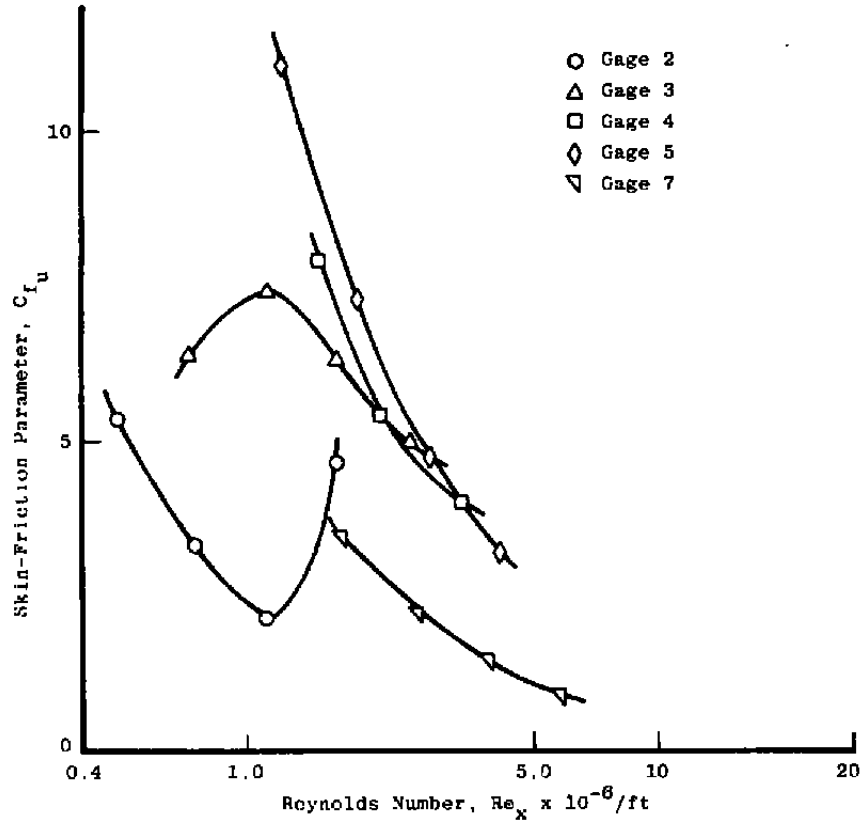

Figure 24. Uncalibrated local skin-friction parameter versus Reynolds number based on distance from nose of the EBOR model.

5.0 CONCLUSIONS

An experimental program was conducted to demonstrate the embedded-wire technique of obtaining local skin friction and to apply the technique to measurements on a model in Tunnel 16T. The experimental investigation demonstrated that repeatable embedded-wire gage data can be obtained if the gages are calibrated in place. In-place calibration allows shifts in calibration constants to be easily corrected by pretest wind-off gage readings. Gage sensitivity is dependent upon the gage temperature differential selected for operation. Therefore, the gages must be operated at the same overheat temperature as the calibration.

Reinstallation of the gages in a model in Tunnel 16T following laboratory calibration caused shifts in the calibration constants that could not be corrected without recalibration. However, by determining new calibration constants in situ, the embedded-wire gages compared favorably with the other skin friction measuring methods. It was also demonstrated that the embedded-wire gages may be used to detect boundary-layer transition

without calibration. This application may require construction of embedded-wire gages that are contoured to the model surface.

Possible improvements in the embedded-wire gage technique include:

1. Developing alternate methods of calibrating the gages in place, or developing gages which retain their calibration when moved from the calibration rig to the model;

2. Shortening the required gage setup time by automating the data acquisition system; and

3. Automatically controlling the gage temperature to adjust for changes in model temperature.

REFERENCES

1. Ludwieg, H. "Instrument for Measuring the Wall Shearing Stress of Turbulent Boundary Layers." NACA TM 1284, May 1950.

2. Liepmann, H. W. and Skinner, G. T. "Shearing-Stress Measurements by Use of a Heated Element." NACA TN 3268, November 1954.

3. Bellhouse, B. J. and Schultz, D. L. "The Measurement of Skin Friction in Supersonic Flow by Means of Heated Thin Film Gauges." Aeronautical Research Council, Reports and Memoranda No. 3490, October 1965.

4. Rubesin, M. W., Okuno, A. F., Mateer, G. G., and Brosh, A. "Flush-Mounted Hot-Wire Gage for Skin Friction and Separation Detection Measurements." 6th International Congress on Instrumentation in Aerospace Simulation Facilities, Ottawa, September 1975.

5. Murthy, V. S. and Rose, W. C. "Buried Wire Gage for Wall Shear Stress Measurements." AIAA 10th Aerodynamic Testing Conference, San Diego, California, April 19-21, 1978.

6. Anderson, C. F., Dougherty, N. S., Jr., and Parker, R. L. "An Experimental Investigation of Techniques to Suppress Edgetones from Perforated Wind Tunnel Walls." AEDC-TR-75-88 (AD-A013728), August 1975.

7. *Test Facilities Handbook* (Eleventh Edition). "Propulsion Wind Tunnel Facility, Vol. 4." Arnold Engineering Development Center, June 1979.

8. Preston, J. H. "The Determination of Turbulent Skin Friction by Means of Pitot Tubes." *Journal of the Royal Aeronautical Society*, Vol. 58, February 1954, pp. 109-121.

9. Benek, J. A. "Effects of Acoustic and Vortical Disturbances on the Turbulent Boundary Layer at Free-Stream Mach Number 0.5." AEDC-TR-77-73 (AD-A047921), December 1977.

10. Whitfield, D. L. "Integral Solution of Compressible Turbulent Boundary Layers Using Improved Velocity Profiles." AEDC-TR-78-42 (AD-A062946), December 1978.

11. Spratley, A. V. "An Investigation of Boattail Geometry and Reynolds Number Effects on Forebody and Afterbody Drag at Transonic Mach Numbers." AEDC-TR-76-161 (AD-A035872) February 1977.

12. Patel, V. C. "Calibration of the Preston Tube and Limitations on Its Use in Pressure Gradients." *Journal of Fluid Mechanics*, Vol. 23, Part 1, 1965, pp. 185-208.

13. Allen, J. M. "Evaluation of Compressible-Flow Preston Tube Calibration." NASA TN D-7190, May 1973.

14. Whitfield, D. L. "Analytical, Numerical, and Experimental Results on Turbulent Boundary Layers." AEDC-TR-76-62 (AD-A027588), July 1976.

15. Fenter, F. W. and Stalmach, C. J., Jr. "The Measurement of Local Turbulent Skin Friction at Supersonic Speeds by Means of Surface Impact Pressure Probes." Defense Research Laboratory Report DRL-392, CM-878, University of Texas, Austin, Texas, October 1957.

16. Holman, J. P. *Experimental Methods for Engineers*. McGraw-Hill Book Company, New York, 1971 (Second Edition), pp. 33-78.

NOMENCLATURE

a	Slope of the temperature-resistance calibration curve, °F/ohm
A	Slope of the embedded-wire shear stress calibration curve, watt-ft$^{2/3}$/°F
A^i	Model surface area for element i, ft^2
b	Zero intercept of the temperature-resistance calibration, °F
B	Zero intercept of embedded-wire shear stress calibration curve, watt/°F
c_p	Specific heat at constant pressure, BTU/lb-°F
C_D	Balance measured total drag force coefficient (Eq. 11)
C_f	Local skin-friction coefficient, (Eq. 7)
C_{f_B}	Total skin-friction force coefficient estimated from balance measured total drag force and integrated pressure drag force, $C_D - C_{DP}$
C_{f_T}	Total skin-friction force coefficient determined from integrated embedded-wire measurements, (Eq. 9)
C_{f_u}	Uncalibrated skin-friction parameter, (Eq. 15)
C_p	Local pressure coefficient, $P\text{-}P_\infty/q_\infty$
C_{DA}	Integrated afterbody pressure drag force coefficient, (Eq. 10)
C_{CAV}	Cavity pressure force coefficient, (Eq. 10)
C_{DF}	Integrated forebody pressure drag force coefficient, (Eq. 10)
C_{DP}	Integrated pressure drag force coefficient, $C_{DF} + C_{DA} - C_{CAV}$
f_i	Local shear stress at location i, lbf/ft^2
F	Total integrated skin-friction force, lbf

I	Current through the embedded wire gage, amperes
k	Coefficient of thermal conductivity, Btu/hr-ft, °F
ℓ	Streamwise dimension of the heated-wire gage, ft
L	Length of EBOR model, 130 in.
M_∞	Free-stream Mach number
M.S.	Model station, in.
N	Integration index equal to the number of embedded-wire gages, (Eq. 8)
Nu	Nusselt number, $q - q_o/sk(\Delta T)$
OD	Outside diameter, in.
P	Local static pressure, psf
P_∞	Free-stream static pressure, psf
Pr	Molecular Prandtl number, $\mu c_p/k$
PT	Tunnel total pressure, psf
q	Heat-transfer rate with flow, Btu/hr
q_∞	Free-stream dynamic pressure, psf
q_o	Heat-transfer rate without flow, Btu/hr
r_i	Model radius at location i, in.
R	Embedded-wire gage resistance, ohms
ΔR	Difference between heated and unheated resistance of the embedded-wire gage, ohms

Re_∞ Free-stream unit Reynolds number, 1/ft

Re_x Reynolds number based on distance from the nose of the EBOR model, $Re_\infty * x$

s Distance between the electrodes of the gage, ft

S Maximum cross-sectional area of the model, ft^2

T Static temperature of the embedded wire gage, °F

ΔT Difference between the heated and unheated temperature of the embedded-wire gage, °F

T_T Tunnel total temperature, °R

V Voltage across the embedded-wire gage, volts

x Axial distance from the nose of the model, in.

λ Equivalent length factor, dimensionless

μ Dynamic molecular viscosity, $lbf\text{-}sec/ft^2$

μ_w Dynamic molecular viscosity evaluated at the wall static temperature, $lbf\text{-}sec/ft^2$

ϱ_w Fluid density evaluated at the wall static pressure and temperature, lbm/ft^3

τ_w Local shear stress at the wall, lbf/ft^2

θ Radial position measured from the top row of pressure orifices, positive clockwise looking upstream, deg